Spring 4-11-2017

ALUMINUM ZINC OXIDE (AZO) OPTIMIZATION PROCESS FOR USE IN OPTICALLY TRANSPARENT ANTENNAS

Maria Elizabeth Zamudio
University of New Mexico

María Elizabeth Zamudio Moreno
_____

Candidate

Electrical and Computer Engineering
_____

Department

This dissertation is approved, and it is acceptable in quality and form for publication:

Approved by the Dissertation Committee:

Christos Christodoulou   , Chairperson
_____

Edl Schamiloglu
_____

Dimitris Anagnostou
_____

Tito Busani
_____

_____

_____

_____

_____

i

ALUMINUM ZINC OXIDE (AZO) OPTIMIZATION PROCESS FOR USE IN OPTICALLY TRANSPARENT ANTENNAS

by

MARIA ELIZABETH ZAMUDIO

B.Sc., Telecommunications Engineering,
Distrital University Francisco José de Caldas, Bogotá,
Colombia,2007
M.Sc. Electrical Engineering
The University of New Mexico, Albuquerque, New Mexico
U.S.A, 2011

DISSERTATION

Submitted in Partial Fulfillment of the
Requirements for the Degree of

**Doctor of Philosophy
Engineering**

The University of New Mexico
Albuquerque, New Mexico

May, 2017

DEDICATION

To my parents Elizabeth and Rafael,

and my sister Paula

who always believed and supported me.

ACKNOWLEDGMENTS

I would like to express my gratitude to my advisor Dr. Christos Christodoulou who gave me great support during my research. I would like to express my thanks and appreciation to Dr. Tito Busani; his knowledge and guidance encouraged me to accomplish successful results. I would like to thank Dr. Edl Schamiloglu, and Dr. Dimitris Anagnostou for their support and supervision. Also, I want to thank all the researchers that helped me during the realization of the research including my lab fellows, and all the members of Dr. Tito Busani's group at CHTM for their contribution and support.

ALUMINUM ZINC OXIDE (AZO) OPTIMIZATION PROCESS FOR USE IN OPTICALLY TRANSPARENT ANTENNAS

by

MARIA ELIZABETH ZAMUDIO

B.Sc. Telecommunications Engineering, Distrital University Francisco José de Caldas, Bogotá, Colombia, 2007
M.Sc. Electrical Engineering, University of New Mexico, Albuquerque, U.S.A, 2011
Ph.D. Engineering, University of New Mexico, Albuquerque, U.S.A, 2017

ABSTRACT

The importance of having an optimal material for fabricating Optically Transparent Antennas (OTAs) is crucial for designing highly efficient antennas that can be integrated with photovoltaics. Transparent Conductor Oxides (TCOs) are promising for OTA fabrication due to their capability of being simultaneously transparent at optical frequencies and conductive within the radio frequency (RF) range.

In this work a new material was developed and optimized to be used for fabricating an optically transparent antenna on a solar cell. Aluminum and Zinc Oxide were co-sputtered onto Si and onto a polycrystalline photovoltaic cell and then annealed between 350°C and 450°C for 24 and 48 h in N2 ambient. The annealing process ensured the formation of the Aluminum Zinc Oxide (AZO) with

a DC conductivity of $3.48 \times 10^5 \, S/cm$ and a transparency of 86% for a thickness between 350 and 750 nm.

This new AZO material was shown to be capable of yielding high levels of conductivity at RF frequencies and excellent transmittance at optical frequencies. The material was tested and validated by performing RF characterization, and by fabricating and testing different optically transparent antennas. The details of the fabrication process, its optimization process, the design of the optical antennas are presented in details and discussed. The material was tested and validated by performing RF characterization, and by fabricating and testing different OTA designs.

Table of Contents

LIST OF FIGURES

LIST OF TABLES

Chapter 1: Introduction

1.1. _Background_

Optically Transparent Antennas (OTAs) can be integrated with any clear substrate and used for different applications, such as vehicular communications, where they can be attached to security glass windows, similar to their implementation of any building's windows. They can also be used on a computer or video monitors, and for integration with solar panels. For the majority of applications, a transparency level above 60% is acceptable; however, for integration with solar panels, they must have a transparency level higher than 80%.

This work has been motivated by the necessity to improve the efficiency of optically transparent antennas in general and, in particular, to integrate them with solar panels. The present work addresses the following:

1) Trade-offs between the transparency and the efficiency of the antenna.

2.) The efficiency of transparent conductive materials.

3.) Integration of optically transparent antennas with solar panels.

4.) Propose and efficient device for energy harvesting (solar energy and RF energy).

These challenges are briefly explained in the next paragraphs.

1.1.1. _Trade-offs between transparency and efficiency of an OTA_

Transparency and efficiency of optically transparent antennas are inversely proportional since when trying to achieve more transparency the antenna efficiency is reduced and vice versa. Over the years, researchers have been trying to optimize the transparency and the efficiency of transparent antennas [1]. They have used mainly two methods: meshed conductors, and transparent conductors.

When using a meshed conductor, the antennas can be fabricated by printing conductive ink on the substrate, or by forming meshes with a traditional conductor, such as copper. Designing antennas with meshed sheets of conductive material facilitate simplicity and lower the cost of the product. The relationship between the width of the mesh, the efficiency of the antenna, and the optical transparency have been shown in a comparative study in [2]. By varying the width and the number of lines of the mesh, efficiency can be improved for a fixed transparency. In the study, an efficiency of 60% was achieved for a fixed transparency of 90%.

In using transparent conductors, different conductive materials have been tested, including ITO (indium-tin-oxide) and AgHT (transparent conductor film based on coated silver). ITO has good RF conductivity and transparency. Nevertheless, the efficiency of antennas made with ITO is only 18% because of the unwanted RF losses due to high skin depth effects at low frequencies [3]. To

reduce the RF losses as well as to increase optical transparency, researchers have used printed antennas made with meshed ITO [4], finding that this technique improves the transparency and efficiency. However, this improvement has been seen only for frequencies higher than 10GHz. Most of the applications for RF harvesting are at lower frequencies, as shown in Figure 1.1. AgHT does not produce a better performance. It has been tested for antenna fabrication [5] and it has been demonstrated that it presents higher losses than ITO. Hence its efficiency is even lower than 18%. The poor characteristics of AgHT and the difficulty of achieving high efficiency for low frequencies with ITO have motivated the search for a new transparent material with excellent optical transparency and RF conductivity that can be efficient at lower frequencies.
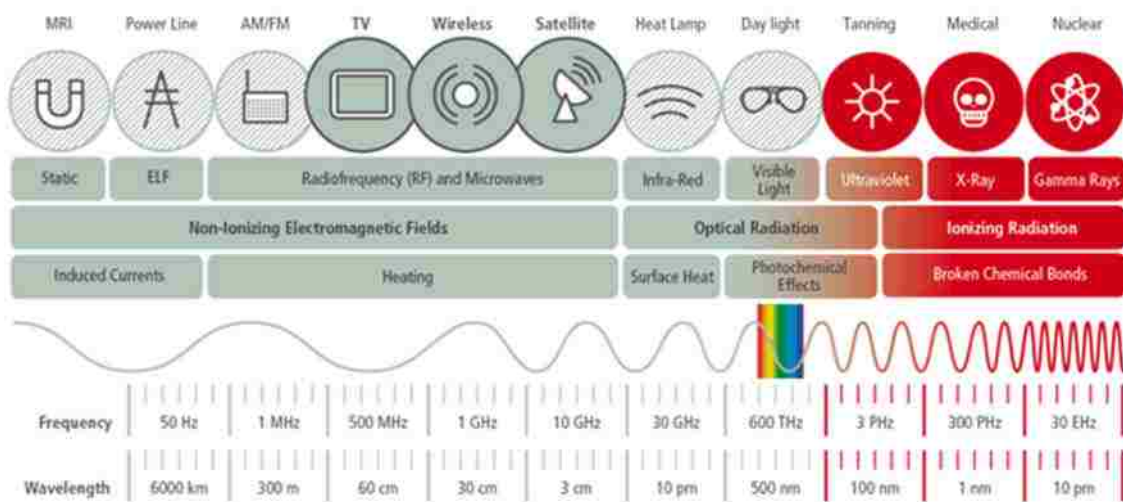
Figure 1.1 Electromagnetic spectrum and its applications [6].

1.1.2. _Efficiency of transparent conductive materials_

Transparent conductive materials have many uses, they have been used as a coating to reflect Infrared IR heat for energy conservation purposes, as a touch screen for flat panel displays (mostly used on ATMs), and as a coating material on solar panels. The most popular transparent conductive material is ITO as previously mentioned, a member of the transparent conductive oxides or TCOs. Although the use of TCOs for transparent antennas has had little application, there has been some research on using transparent antennas on vehicle windows and on solar cells [7, 6]. The research has shown, however, that the efficiency of the antennas is less than with traditional conductive materials. Moreover, there has not been enough understanding of the antenna efficiency for a broad range of frequency bands, of its relationship with the conductivity range, and of the transparency that should be expected from available TCOs.

It is necessary to appeal to the knowledge of materials engineers to clarify the efficiency of the antenna and its relation to the transparency and the conductivity of TCOs. By doing this, the process for transparent conductive materials can be optimized to achieve the highest efficiency when used for transparent antenna applications. As mentioned before, the use of ITO produces a high level of transparency and RF conductivity; however, research with this material is becoming difficult due to the risk of its depletion which has led to high cost. This high cost has resulted in the investigation of alternative materials. The work in this dissertation describes research focused on the optimization of Aluminum Zinc Oxide (AZO). AZO presents many advantages:

a) It has more conductivity than previous materials like AgHT,

b) it has high transmission in the visible region, and

 c) it has no risk of depletion which translates to cost efficiency.

1.1.3. *Integration of optically transparent antennas with solar panels*

The reason for obtaining the best performance from a transparent conductive material is to be able to integrate an OTA on top of a solar panel without degrading the light absorption of the panel. Subsequently, by attaching a rectifier circuit to the resulting device, two different types of energy can be harvested: Solar energy, and RF energy. This concept is useful especially in cases when light or sun energy is not available. Figure 1.2 shows the integration of OTAs with solar panels, for combined RF/Solar energy harvesting.
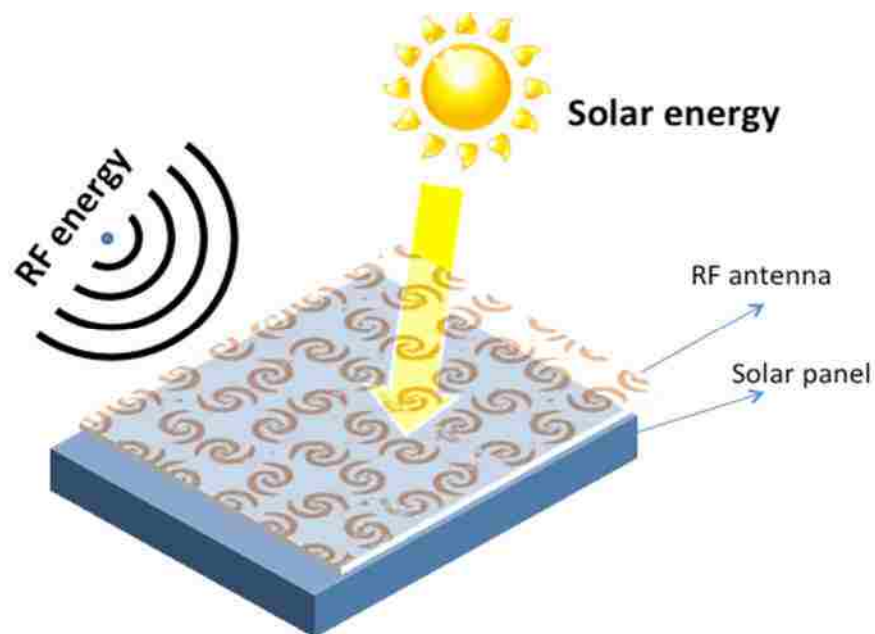
Figure 1.2 Schematic of the integration between optically transparent antennas and solar panels.

Additionally, this technology can significantly reduce volume, cost, and weight when used for applications on small satellites; moreover, the optimization of the transparent conductive material will allow designing of more antenna systems such as antenna arrays that provide higher gain, and hence higher efficiency.

1.1.4. *Efficient harvesting energy (solar energy and RF energy).*

The available solar energy reduces depending on the intensity and absence of light; this occurs during night hours and especially during nights with no moon. In order to efficiently harvest energy during these hours it is proposed to integrate an antenna with a solar cell; since the power of the available RF energy is much lower than the power from solar energy, it is important for this antenna to have high efficiency and to be compatible with solar cell technology without decreasing its effectiveness.

The purpose is to integrate a highly efficient optically transparent antenna for RF harvesting on top of a solar panel without affecting its light absorption. The device will absorb the ambient RF energy existing in the environment using the transparent antenna, and solar energy using the solar panel. When a rectifier circuit is added to the design, the absorbed energy in the form of waves, can be transformed into direct current (DC) that can be stored and can be used to feed small electrical devices.

1.2. *Energy Harvesting*

Energy surrounds us in different forms in our everyday life. The energy is presented as thermal energy, as solar energy, as wind power, as mechanical energy, and as electromagnetic energy. The energy from these sources sometimes does not provide enough power. This means that these sources are not able to deliver sufficient energy for some specific purposes. When this happens, it is necessary to capture the energy by means of a harvester, and store it until it can be used for the final applications [8]. The main sources of energy that this work focuses on are:

- Electromagnetic Energy: Electromagnetic energy propagates through the space as radiation, and it has different forms: Radiated heat, visible light, radiofrequency, X-rays or Gamma rays;

- Photonic Energy: Or solar energy, from solar light, artificial light, and interior light in buildings.

Table 1.1 presents a comparison between the available power from the energy sources: Sun, thermal, vibration, and RF; and they are compared with their harvested power. [9]

Table 1.1 Comparison available vs. harvested power.

Source		Power at the source	Harvested Power
Light	Outdoor	$100mW/cm^2$	$10\ mW/cm^2$
	Indoor	$0.1mW/cm^2$	$10\ \mu W/cm^2$
Thermal	Human	$20\ mW/cm^2$	$30\ \mu W/cm^2$
	Machine	$100\ mW/cm^2$	$1\text{-}10\ mW/cm^2$
Vibration/motion	Human	$0.5m$ at 1 Hz	$4\ \mu W/cm^2$
		$1m/s^2$ at 50 Hz	
	Machine	$1\ m$ at 5 Hz	$100\ \mu W/cm^2$
		$10\ m/s^2$ at 1 kHz	
RF	GSM BSS	$0.3\ \mu W/cm^2$	$0.1\ \mu W/cm^2$

The harvester's ability to 'scavenge' energy plays a significant role. This device must first capture the available energy with specific sensors, for instance, to capture mechanical energy by vibration, there are used piezoelectric materials which can generate electricity when exposed to mechanical stress, their functionality is based on the piezoelectric phenomenon discovered by Pierre and Curie back in 1880. [10].

Moreover, a harvester must be able to manage a broad range of voltage and currents, including overcharge and overvoltage, also waveforms and variable input conditions.

1.3. _RF Harvesting_

One of the the main topics for this research is obtaining highly efficient RF energy harvesting antennas. In the following paragraphs, RF energy is defined as well as the types of sources that generate it and the available power that can be extracted from it. This RF energy is the type of electromagnetic energy that is present in the radio frequencies of the electromagnetic spectrum (3Hz to 300GHz).

1.3.1. _Residual RF available energy_

In order to identify how much energy can be harvested, the first step was to know the available ambient average power. For this purpose, an experiment was set with the Agilent PXA N9030A signal analyzer and a Double Ridge Guide Horn Antenna SAS-571 within a frequency range between 700 MHz to 18 GHz.

The aim of the experiment was to measure the incoming power of the antenna during a 24-hour period. A remote connection was used to control the PXA. The Matlab code in Appendix A was generated to automatically communicate with the PXA and save the obtained data every 20 minutes during the established period. The generated files were analyzed, and the average power was obtained. Figure 1.3 shows the plot obtained with the measured results.
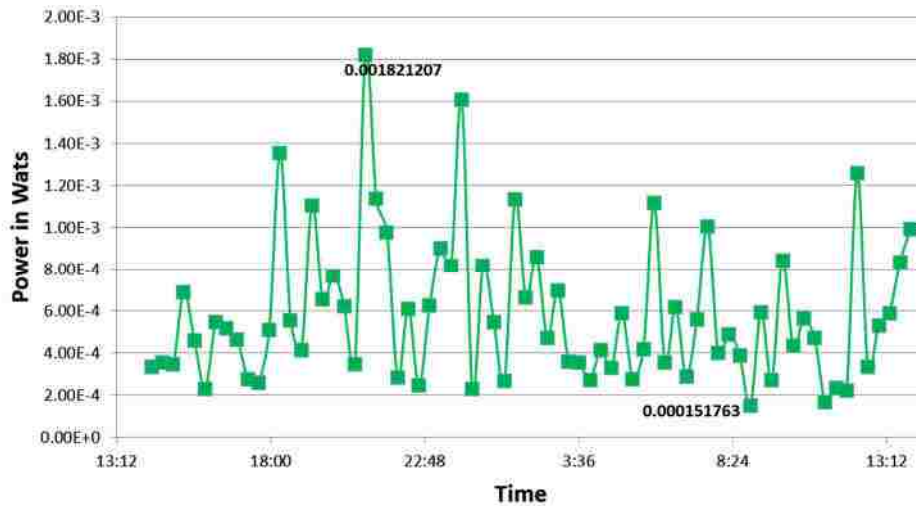
Figure 1.3 Average power measured during the 24-hour period.

The plot shows the maximum peak to be at 8:57 p.m. with a value of $P = 1.821207mW$, and the minimum at 8:57 a.m. with a value of $P = 0.151763mW$. Once these values are known, the parameters for the RF energy harvesting device can be optimized to harvest energy in the most efficient way.

Figure 1.4 shows a diagram of the harvesting device, the typical components of a harvester are a receiving antenna, a rectifier circuit, a storage and management, and a load.
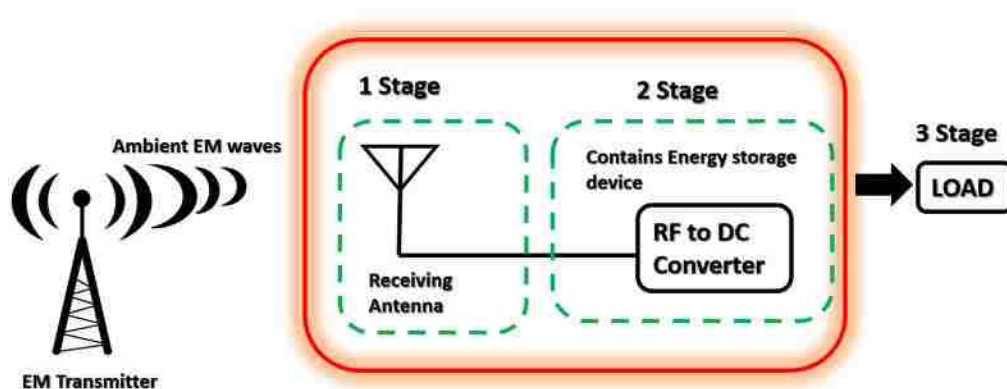
Figure 1.4 Typical RF harvester diagram.

The receiving antenna absorbs the available ambient RF energy; this antenna should have good efficiency to be able to absorb most of the low power RF energy available. The energy absorbed by the antenna is in the form of electromagnetic waves and since these waves present alternative periods or Alternating Current (AC), it is necessary to transform this power to direct current (DC) to be able to charge small electronic devices. The conversion system from AC to DC is called *rectification*. The core of the rectification process is a diode, and a simple way to achieve this rectification is to employ a single diode rectifier. In the single diode rectification approach, the diode lets current flow only in one direction, that is, it allows only half of the AC wave to pass to the load. This simple rectifier is called half-wave rectifier. Figure 1.5 shows a half-wave rectifier.
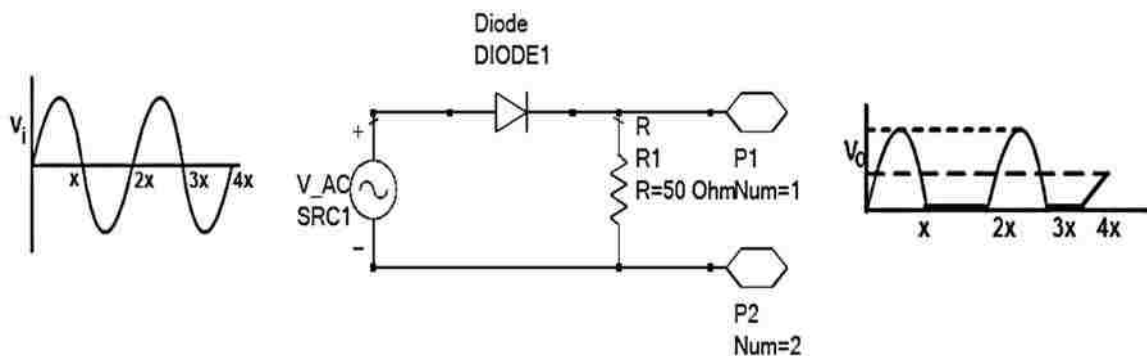
Figure 1.5 Half-wave rectifier.

A more complex but more efficient way to achieve rectification is to use a full wave rectifier since it rectifies both halves of the wave, thus becoming a more efficient rectifier [11]. The most widely used options for obtaining full rectification, are achieved by either employing two diodes connected to a center tap of a transformer, or by using a four-diode bridge which does not require a

transformer. Figure 1.6 depicts the two types of a full wave rectifier, a) two diodes connected to a transformer, and b) a four-diode's bridge [11].
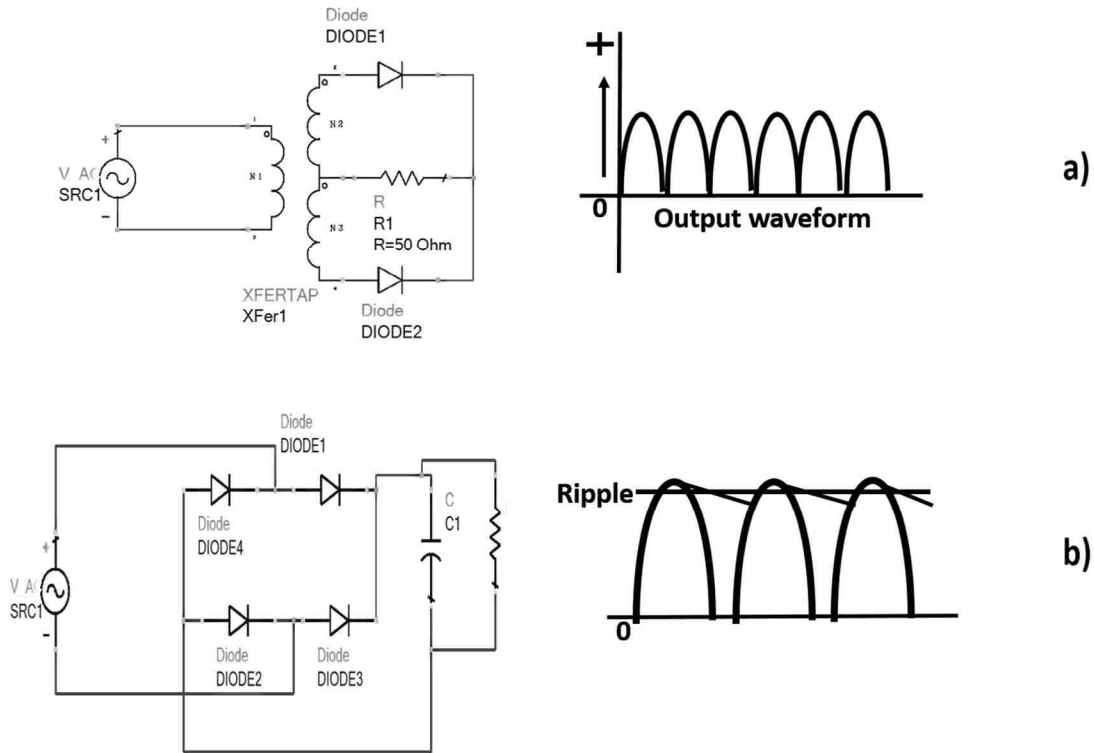
Figure 1.6 Full wave rectifiers.

The efficiency of a rectifier circuit depends on the matching between the input power and the load. If the diode's input power is lower than its junction voltage, the diode will not perform as a rectifier. Therefore, it is important to design a suitable rectifier circuit that can rectify with low input power, that means there must not be mismatches between the input power and the load.

Having an efficient rectifier does improve the harvesting capability of an antenna itself, and it does guarantee that the incident wave is efficiently converted to DC power. Since the residual RF energy power is typically low, the

input power at the rectifier is usually in the order of $Pi \approx 10\mu W$. In this situation, the efficiency of the system might be affected if the rectifier circuit is simply connected to the load. In order to avoid any decrease on efficiency, the rectifier is connected to a power management phase which contains a power amplifier. When the stored energy is sufficient, a storage device consisting of a battery or a capacitor is needed to keep the energy stored and delivered to a small device.

In conclusion, an application of optically transparent antennas is very attractive in terms of integration with for solar energy harvesting devices. An efficient integration of RF optically transparent antennas with solar cells improves energy harvesting by allowing for harvesting energy during no sunlight hours. Moreover, this integration brings not only a backup system for solar energy harvesting with RF energy harvesting but also, the opportunity of use this technology for more applications, such as vehicle communications, space communications, and even self-powered communications systems for satellites and space power beaming.

1.4. *Dissertation Structure*

This dissertation consists of five chapters:

Chapter 1 Introduction: The main topic of this Ph.D. dissertation is introduced and briefly discussed in this section including the concept of RF energy harvesting, the major approaches to the research are presented as well.

Chapter 2 Background on Optically Transparent Antennas: This chapter explains in detail what are transparent conductive materials, their properties and their feasibility for use in different applications. A review of optically transparent antennas and the state of the art research in the area are presented in this section.

Chapter 3 Why Aluminum Zinc Oxide? The optimization process of AZO films is described, the details of the fabrication and characterization processes are explained, and all results are summarized.

Chapter 4 Antenna Designs, fabrication process, experiments, and data: The viability of integrating optically transparent antennas made with AZO films on top of solar cells is investigated. The fabrication process of different antennas as top contacts of solar cells and their results is presented in this part of the document. Applications and different antenna systems designed with AZO material are presented.

Chapter 5 Conclusions and future work: Final results are discussed and proposed future research ideas are presented and discussed.

Chapter 2: Background on Optically Transparent Antennas

In this chapter the concept of optical transparency as well as the principles of transparent materials are explained. The state of the art for OTAs is introduced, their variations regarding materials and fabrication techniques, including the challenges associated with designing this type of antennas are also presented and discussed.

2.1. *Optical Transparency*

Optical materials depending on their interaction with visible light can be classified into three groups:

- *Transparent*: Materials that can transmit light with low absorption and reflection;

- *Translucent:* The transmission of the light through the material is diffused;

- *Opaque*: This kind of materials are impermeable to the transmission of light which means that the energy of the photons is absorbed.

Materials can be opaque and transparent depending on certain optical properties.

2.2. *Optical Materials*

An optical material, can be utilized in a variety of applications [12]. The applications where an optically transparent material can be used depend on different optical phenomena that are described below.

Luminescence: This phenomenon explains the emission of light from relatively cold materials. When a proper material is excited by a source such as: X-rays, chemical reactions, or electron beams, it instantly emits visible radiation. This kind of emission is called fluorescence if it happens after 10^{-8} secs of being exposed to the source. If this emission takes more than 10^{-8}s it is called phosphorescence. The intensity of luminescence is given by [12]:

$$I = I_0 \exp\left(-\frac{t}{\tau}\right) \tag{2.1}$$

Lasers: The light amplification by stimulated emission of radiation, is an amplification of photons. When specific materials are excited they produce photons that also excite more photons. Lasers are monochromatic because in the emission process photons stimulate more photons with the same wavelength; this makes them also coherent which allows a laser to be fine focus as well.

Thermal Emission: The process of heat emission is when the electrons that are excited to the higher-level release photons, this happens because of the rise of the temperature of the determined material. The higher the temperature, the wider the range of the emitted wavelengths. This range of wavelengths starts

from the longest which is infrared rays, passing through the visible light and the shortest is ultraviolet rays.

Photoconductivity: It is the increase in the electrical conductivity of a particular material when exposed to light. Usually, that material is a crystalline semiconductor. The type of semiconductor that is highly photoconductive is typically made of cadmium sulfide CdS, lead sulfide PbS, silicon Si, and germanium Ge. In the process of photoconductivity, the intensity of the impinging photons should be the same or greater than the band gap of the material; when this happens, pairs of electron-hole are created generating current.

It has been shown that the optical transparency of a material depends on its optical properties, and, on its interaction with light. Table 2.1 shows a list of the index of refraction for different materials, their reflectivity, and their absorbance. The less reflectivity and absorbance a material has, the higher is its transparency level.

Table 2.1 Values for index of refraction, absorbance and reflectivity for different materials [13].

	Material	η	Absorption (cm^{-1})	Reflectivity
Metals	Aluminum (Al)	1.2667	1.446e+6	0.91287
	Copper (Cu)	0.307	6.8204e+5	0.90906
	Gold (Au)	0.19609	6.4654e+5	0.93480
	Silver (Ag)	0.15677	7.554e+5	0.96034
Crystals	Diamond (C)	2.4105	0.0000	0.17105
	Germanium (Ge)	5.4717	1.624e5	0.4851
	ICE (H2O)	1.3084	0.00216	0.017853
	Silicon (Si)	3.8774	196.10	0.34804
Glasses	BK7 optical glass	1.5151	0.00240	0.041943
	Soda lime clear	1.5216	0.14196	0.042791
	Soda lime green	1.5216	0.62988	0.042791
Liquids	Water (H2O)	1.3317	0.0029152	0.020236
	Mercury (Hg)	1.9799	1.0387e6	0.78145

These values are for the 632.8 nm wavelength, this corresponds to the range of red color, which possesses the longest wavelength of all the colors in visible light.

2.3. _Transparent Conductors_

Transparent Conductors or TCs as referred for the rest of this document, are materials that have the dual characteristic of being conductive and transparent in the visible range simultaneously. This is accomplished by highly doped wide band gap oxides. For instance, in In_2O_3, SnO_2, and ZnO, the band gaps of these oxides prevent interband optical excitation for visible light due to their wide bandgaps, and thus, their electrical conductivity is achieved due to the high carrier concentrations achieved by doping, typically in the range of 10^{20}-$10^{21} cm^{-3}$ [1].

TCs are built with a variety of materials including metals, ceramics, glass, plastics, molecular and polymer organics, and semiconductors. These types of materials have low-emissivity windows, consequently, they reflect infrared thermal heat allowing the creation of energy conservation windows. Energy conservation windows are utilized in ovens to conserve energy, and to keep the outside temperature safer to touch. Moreover, the electrical conductivity of transparent conductors has been employed in surface electrodes that go on flat panel displays and on solar panels [14].

TCs are used as optically transparent contacts for a wide variety of applications. These materials have been used for smart windows to maintain display cases frost free by incorporating the TC with an electrochromic material to defrost the displays. TCs also have been employed in xerographic copiers to dissipate static electricity. Furthermore, they can also be employed as contacts

on glass touch-control panels, as invisible security circuits on windows, and as transparent antennas for vehicles.

Research on TCs started with Karl Bädeker. In 1907 a paper was published [15] describing the first film-fabrication method of a number of metal compounds: AgI, Ag_2S, Ag_2Se, CdO, CdS, CdSe, CuI, Cu_2O, CuO, CuS, Cu_2S, CuSe, PbO, PbS and TIS . The reported method used sputtering of metallic thin films on glass or mica. In order to find the thickness of the films Bädeker used the weights of the compound and the substrate; then, he removed the thin film, and he measured the substrate weight. With this method, Bädeker had a precision of 2nm. For copper iodide CuI, he assumed an index of refraction of n=2 and predicted its thickness depending on the color of the dielectric. Bädeker also characterized the electrical conductivity of the films using a Wheatstone bridge, and pressing the film with contacts; he also used a meandering current path to reduce the contact phenomena [16].

The investigation on transparent conductors continued through the 1920's. Different glass companies started to file patents about conductive SnO2 (stannous oxide or Tin II oxide) by the 1930's until the 1940's. In 1951 the first patent related with ITO was filed by Corning, and it was about Si-doped In2O3. In 1959, R Arneth,   at the University of Erlangenin Germany described the properties of zinc oxide ZnO. In 1971, in Japan, patents were filed for ZnO varistor and TCO films [17].

AgHT (Silver coated polyester film), has also been used as a transparent conductor as well [18] [19]. This AgHT film has the silver conductive layer in

between two layers of tin oxides and coated with Polyethylene Terephthalate (PET) with a sheet resistance of 4.2 Ω□ [20]. This material has been tested, yet its electrical properties are poor which makes it not suitable for efficient designs of OTA's [21].

Transparent Conductive Oxides (TCOs) are transparent conductors whose absorption of electromagnetic waves is low in the visible region, meaning that they are able of being both conductive at RF frequencies and transparent at the visible region simultaneously. TCOs are typically composites in which the non-metallic portion is oxygen [22].

Although the research on transparent conductive films started before the 1950's, it was not until the last twenty years that transparent conductive oxides became the focus of new applications. The developments of the last couple of decades lead to a significant increment in the number of applications for TCOs, applications such as LCD, plasma, electroluminescence TV, mobile phones display, ATMS, among others are commonly seen and used nowadays [17].

First studies in transparent conductive oxides TCO demonstrated that thin oxide films were more stable for electrical conductivity and electrical transmission than the ones based on metals. The basic requirements for high quality TCOs are:

- A reasonably wide band gap;
- interband transitions >3.1 eV, and
- the ability to donor or acceptor dope to 10^{21} cm^{-3} [23] .

Figure 2.1 shows the band structure of undoped TCO. The Figure also illustrates the shift in the band when is doped, the areas in blue denote the occupied states.
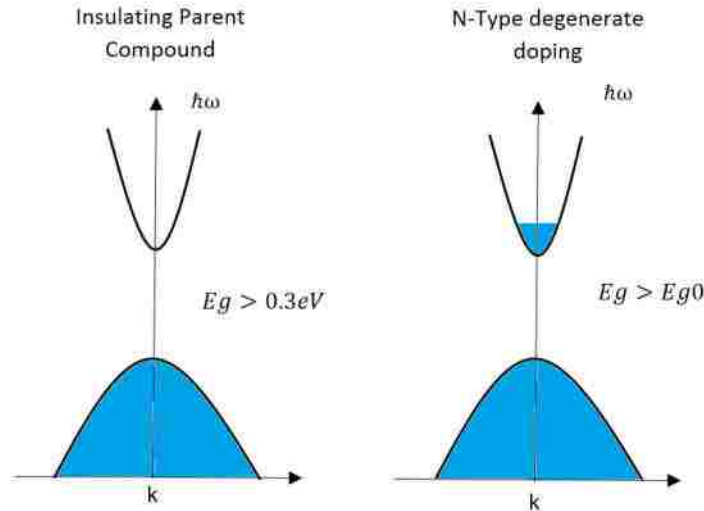
Figure 2.1 Undoped TCO (left), effect of doping (right).

For the case of solar cells the TCO's that are used are the n-type [24]. The most widely utilized TCO for this application is ITO followed by Al: ZnO (AZO). Research has been done on which they employ ITO for optically transparent antennas integrated with photovoltaics [24]. In these studies, the researchers have used ITO films and meshed ITO.

The best optical properties of a TCO (highest conductivity, highest transmission) have been found in composites based on tin oxides doped with indium, and zinc oxides. Indium-tin-oxide or ITO's high conductivity is due to its low resistivity, around $10^{-4}\Omega$*cm [25], and its transmittance has been reported to be about 90.2 % [24]. For the case of zinc oxides, the films with the best optical properties are the ones doped with aluminum. These films possess high conductivity comparable with ITO, in the order of $10^{-4}\Omega$*cm, and high transmittance: T ≈ 90 % [26].

Even though ITO appear to be the most outstanding of the TCO's, the scarcity of indium has increased the cost of its usage as the material of choice. Additionally, ITO is not stable and its electrical properties are affected under special atmospheric conditions were oxygen is removed to prevent oxidation; these atmospheric conditions are called reduced atmosphere, and are used in annealing ovens where it is necessary to prevent corrosion on the metal by avoiding oxygen or any oxidizing vapor. Lastly, indium has a certain potential level of toxicity that represents a hazard to humans and the environment in general [27].

Therefore, to avoid hazards, high costs, and degradation it is necessary to employ other compounds for TCO applications. Some studies employed different materials [27] based on different oxides such as Zn_2SiO_4, $ZnSiO_3$, $MgIn_2O_4$, $Zn_2In_2O_5$, and ZnO multicomponent compounds: $ZnO-In_2O_3$, $MgIn_2O_4-Zn_2InO$. It was shown that the properties of these materials can be controlled by altering their chemical composition. When compared with ITO, films based on ZnO show more stability. They are also more cost effective than ITO and with similar optical properties.

2.4. *Review of OTAs*

Optically transparent antennas present a certain transparency level in the visible region. There exist different ways to achieve an optical transparency level in antennas. One way is to use copper mesh for the antenna geometry, and

another way is to use transparent conductive materials. In this section, these two different ways and a brief literature review of OTAs are presented and discussed.

A chronological review made in Brunel University by Thomas Peter [19] points out that the research on transparent antennas started in 1997 when NASA engineers Rainee N Simons and Richard Q Lee studied transparent patch antennas and compared their performance by using microstrip feeding versus probe feeding. In their experiments, they used a thin film of clear polyester with silver conductor coated with tin oxide: AgHT-8.   The antennas designed were narrow band patch antennas for 2.3 GHz and 19.5 GHz. According to their experimental results, the antennas presented good radiation patterns and input impedance match. Figure 2.2 shows their antennas.
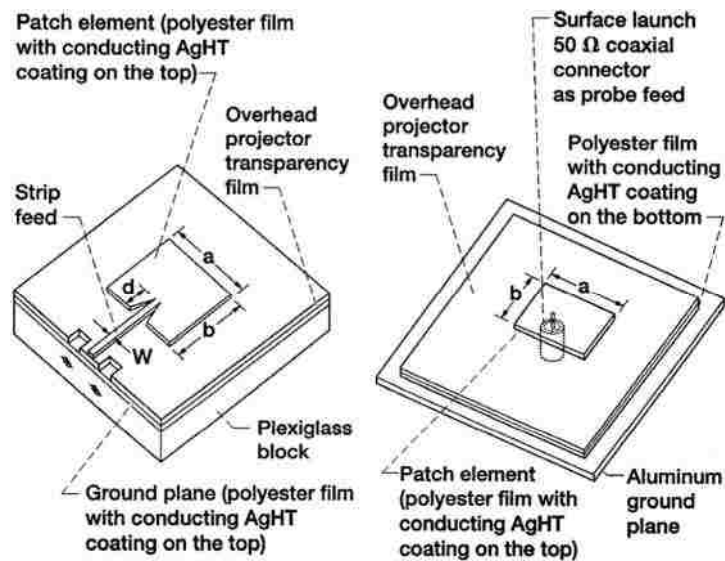
Figure 2.2 Transparent patch antenna (a) microstrip line feed, a=53 mm, b=37 mm, d=8 mm, w=2 mm (b) probe feed, a=9 mm, b=7 mm [28].

Later, different conductive materials were tested for the fabrication of optically transparent antennas. In [17] [29] the authors used gold (Au), aluminum (Al), silver (Ag), Indium-Tin-Oxide (ITO), and compared the results with antennas fabricated with copper (Cu) and a thin aluminum (Al) film. As a conclusion, the authors stated that the most suitable conductors for optically transparent antenna fabrication are gold and silver since the measured results were closer to the results of a dipole antenna made of copper. Figure 2.3 shows the geometry of the antenna and Figure 2.4 shows a plot comparing the transparency level for the different materials. It is noticeable that the degree of transparency in the visible region range (400–700 nm) is good for ITO, close to 80%, and silver and gold are close to the ITO's level. In the case of silver, it is close to 80% for lower wavelengths, 450 to 550 approximately, while for gold it is close to 80% for higher wavelengths, i.e., 550 to 650 approx.
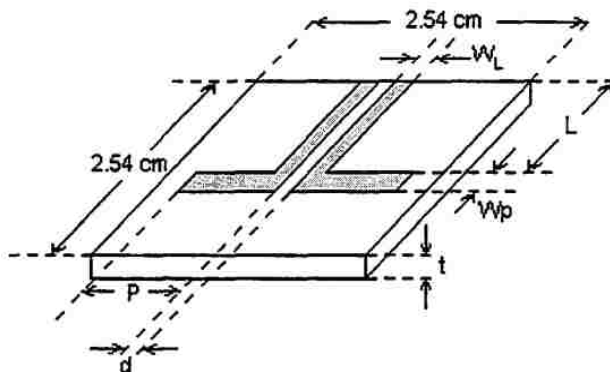
Figure 2.3 Geometry of the antenna [29].
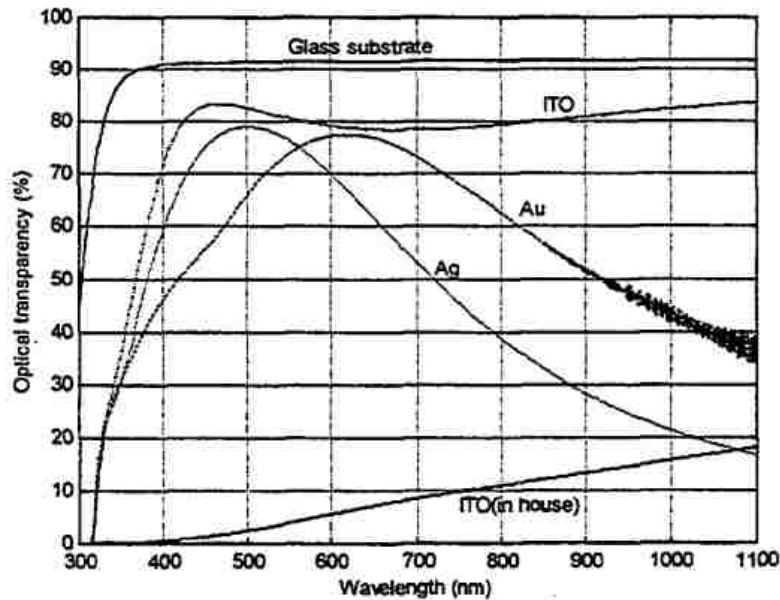
Figure 2.4 Comparison of optical transparency for different materials [29].

In 2006 researchers from National Cheng Kung University in Taiwan [30] designed a transparent monopole antenna, and fabricated a prototype using thin PET coated with ITO. The antenna was a dual frequency antenna for 1.95 GHz, and 5.58 GHz for WLAN (wireless local area network) and WCDMA (wideband code division multiple access). Figure 2.5 (a) shows the geometry of the antenna which has two rectangular slots for impedance matching and is fed with a SMA connector. The ITO film had a thickness of approximately 0.1 mm, and as shown in the picture, there was a space between the radiating patch and the ground plane of 8 mm. Figure 2.5 (b) shows the fabricated prototype.
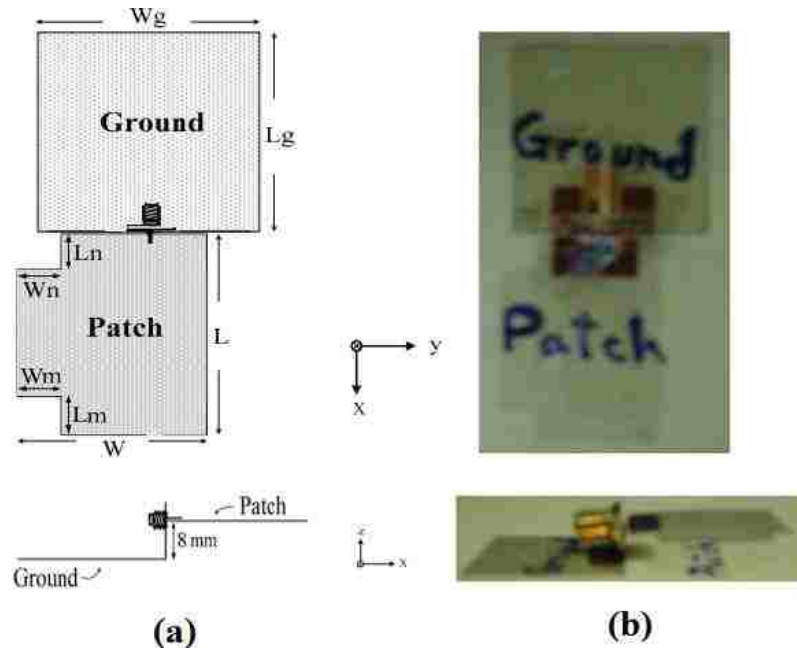
Figure 2.5 (a) Geometry of the total antenna dimension for the patch, and (b) fabricated prototype [30].

In 2007 in Thailand [31] researchers developed a similar transparent antenna by also employing ITO deposited on PET. The antenna was a center fed square patch with dimension 10 by 10 cm. Although the antenna did not reach the <-10 dB for conventional acceptable return loss, the researchers compensated this with an amplifier circuit. The frequency of operation was up to 2.5 GHz and the thin film had a transmittance close to 90% in the visible region.

Similar work was published by the researchers in Japan, during the same year [32]. They fabricated a monopole antenna with ITO and FTO (fluorine-doped tin oxide) which geometrically consisted of a half of a bowtie mounted over a full ground plane as depicted in Figure 2.6 ITO and FTO were deposited on a glass substrate. The results show that a transmittance of 95% for a wavelength of 550nm was achieved. The antenna was designed to work at 2.4 GHz with a gain

of 0.2dB to 4.4 dB, and an efficiency that varied from 46% to 93% depending on the thickness for ITO which alters the film resistance as well.
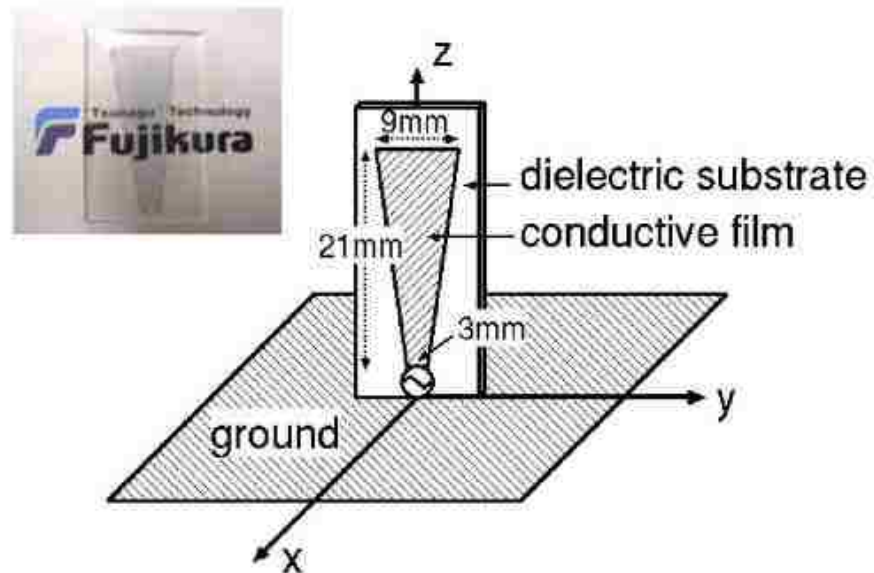
Figure 2.6 Fujikura half bowtie transparent antenna description [32].

In 2009, a paper on "Optically Transparent Conductive Polymer RFID Meandering Dipole Antenna" [33]   presented the design of a transparent meandering antenna for RFID applications. The antenna was made with copper conductor, and with a conductive polymer using PET as a substrate for the antenna. The antenna was designed to work at 900MHz but was not completely transparent, as seen in Figure 2.7 (a). The initial design was a λ/2 dipole, as shown in Figure 2.7 (b), to work at the same frequency, but the size is not useful for RFID applications.
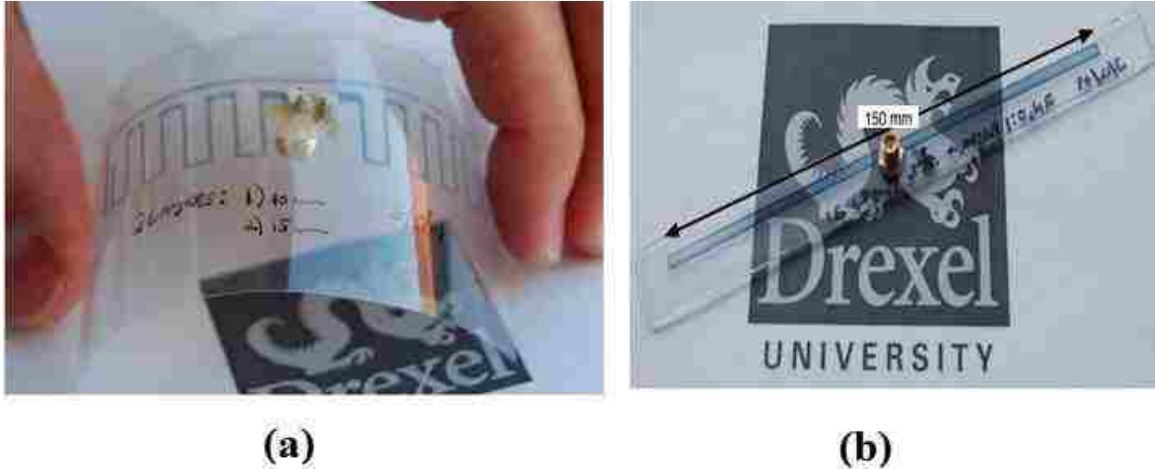
Figure 2.7 Transparent antennas Drexel University 2009 [33].

In 2009, in [18], an UWB antenna design made of transparent conductor, and based on a silver coated film AgHT-4 was introduced. The conductor film AgHT-4 was placed between a glass substrate and an acrylic glass (Perspex) superstrate in order to improve the antenna efficiency. However, this antenna was not completely transparent because it was fed with an aluminum strip. Figure 2.8 shows the structure of the antenna which consists of a monopole disc fed with a CPW (coplanar waveguide), operating from 1 to 8.5GHz.

Figure 2.8 Monopole disc CPW fed antenna [18].

In [34] , An optically transparent monopole antenna with high radiation efficiency manufactured with Silver Grid Layer (AgGL) was presented. The antenna consisted of meshed silver/titanium layers printed on a glass substrate. In this case the transmittance level reached by this meshed antenna was 81.3% in the visible region. Figure 2.9 depicts the meshed antenna.
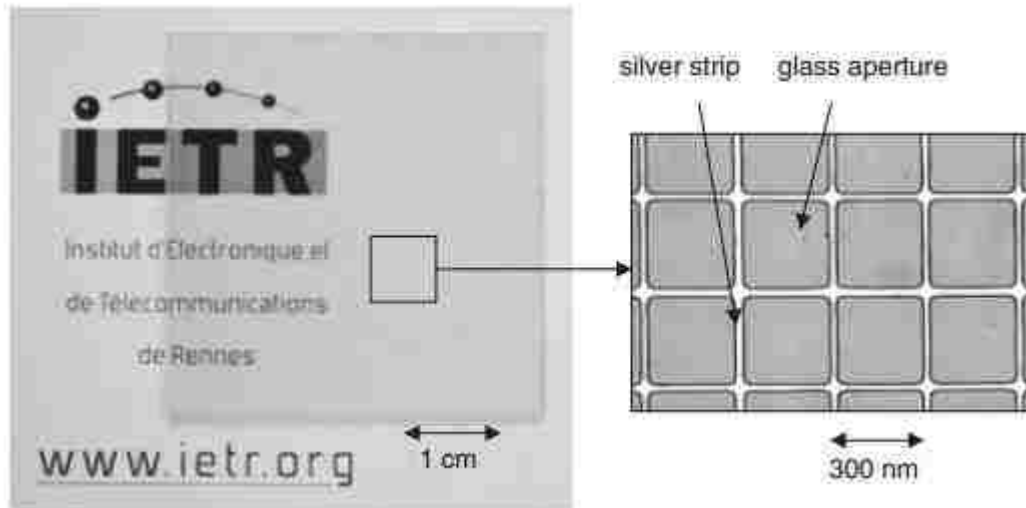
Figure 2.9 Ag/Titanium meshed antenna [34].

In 2010, in a thesis at the University of Utah [35], a copper meshed planar antenna was proposed as an optically transparent antenna since light can pass through the holes of the mesh. The antenna is better in terms of efficiency and in gain compared to previous designs based on TCO due to the high conductivity of copper. However, in this case, there is still the trade-off between transparency and efficiency. When trying to make the mesh lines thinner, the antenna becomes more transparent, but the efficiency decreases since the antenna becomes less conductive. The proposed antenna is shown in Figure 2.10. It can

be seen that the feeding of the antenna is a solid microstrip line which lowers, even more, the transparency level of the overall antenna structure.
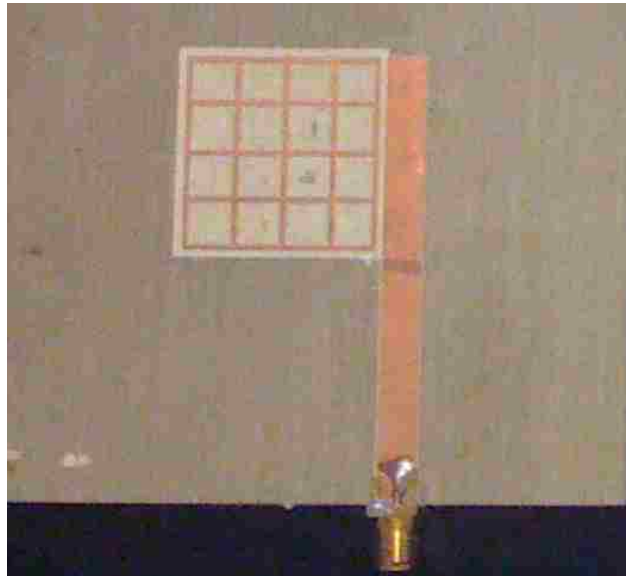
Figure 2.10 Fabricated copper meshed optically transparent antenna [35].

Finally, another transparent antenna made of AgHT in [36], was deposited on top of a solar module covered with glass, fed using an electromagnetically–coupled microstrip copper line, and a superstrate of Perspex. The efficiency of the antenna decreased when the copper feeding line was replaced with a transparent conductor having a gain of -0.8dBi. However, when a copper line was used without the Perspex material the gain was reduced to -2.5dBi, meaning that the superstrate is crucial in increasing the gain of this type of material. Figure 2.11 shows the proposed antenna in [36].
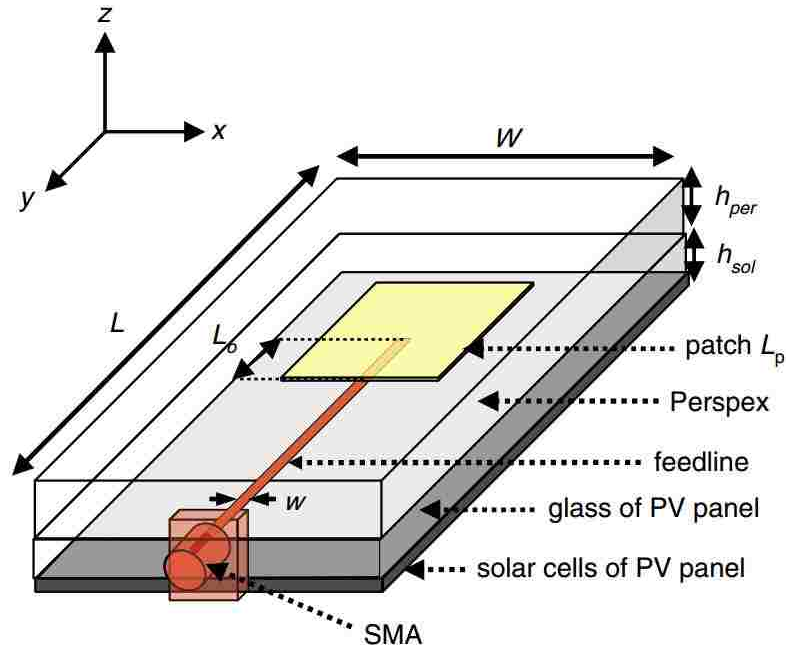
Figure 2.11 AgHT-4 proposed antenna in [36].

2.5. *Challenges of OTA's*

When designing and fabricating antennas, there exist number of trade-offs, namely, gain vs. bandwidth, coupling vs. size, and matching among others. Moreover, the fabrication process can also be challenging. For the case of optically transparent antennas, the design and the fabrication processes face more challenges than the average planar antenna, especially when achieving a high level of transparency. In this section, these different challenges are explained as they are related to the requirements for TCO to be employed for antenna design, the skin depth, the deposition process, and lowering the surface resistance of the material to improve conductivity.

For an antenna to be optically transparent a minimum of 80% transmission in the material is required. The existence of high transparency and high conductivity in transparent oxides is possible due to the laws of physics. This characteristic is because of the mobility of electrons and the carrier concentration in the TCO materials. The electron mobility can be controlled by changing the oxygen and the argon concentrations, and combined with an annealing process electron mobility can be improved as well [2]. In order to understand the physics of transparent conductors it is useful to refer to the Drude model.

One aspect of applying the Drude model for electrodynamics equations is that the values of the mass of the particle have to be altered so that the electrons can be treated as nearly free carriers. With this assumption, the effective mass of an electron in a band becomes the altered value m*, so for a given E and k this becomes [2]:

$$m^* = \hbar \Big/ \frac{d^2 E}{dk^2},$$
(2.2)

This value is found in the literature to be [37]

$m^* \cong 0.35 m_e$.

The conductivity and the permittivity of the TCO can be modeled by Maxwell's equations. In this case the conductivity is expressed as:

$$\sigma_d = \frac{1}{(1 + j\omega\tau)} \qquad \tau = \varepsilon/\sigma \qquad (2.3)$$

Combining the conduction current σ_{DC} and the displacement conductivity σ_d we get:

$$\sigma(\omega) = \left(\frac{N_e q^2 \tau}{m^*}\right)\left(\frac{1}{1 + j\omega\tau}\right) = \frac{\sigma_{DC}}{1 + j\omega\tau} \qquad (2.4)$$

Where:

N_e : TCO electron density

q: Electron charge

Using Maxwell's equation $\nabla \times H = J + j\omega\varepsilon(\omega)E$ we can include the frequency dependency of the dielectric. If we separate the real and imaginary parts for ε we get:

$$\varepsilon_1(\omega) = \varepsilon_\infty - \frac{\omega_p^2 \tau^2}{1 + \omega^2\tau^2} \; and \; \varepsilon_2(\omega) = \frac{1}{\omega}\left(\frac{\omega_p^2 \tau}{1 + \omega^2\tau^2}\right) \qquad (2.5)$$

ω_p : Plasma Frequency

ε_∞ : Relative permittivity in High Frequencies

When $\varepsilon_1(\omega_p) = 0$ then:

$$\omega_p = \left(\frac{N_e q^2}{\varepsilon_\infty \varepsilon_0 m^*} - \frac{1}{\tau^2}\right)^{1/2} \qquad (2.6)$$

To improve the transmission, the plasma frequency ω_p must be much lower than the lowest visible wavelength $\approx 400nm$. When ω_p is just slightly lower than 400nm, the electron density N_e must satisfy 2.7:

$$N_e < \frac{4\pi^2 \varepsilon_\infty m^*}{\mu_0 q^2 \lambda_{visible}^2} \qquad (2.7)$$

In order to define the transmission of TCO's we must know the reflection power which is given by equation (2.8):

$$R(\omega) = \left| \frac{\sqrt{\varepsilon(\omega)} - 1}{\sqrt{\varepsilon(\omega)} - 1} \right|^2 \qquad (2.8)$$

Now, the transmission is:

$$T(\omega) = 1 - R(\omega) \qquad (2.9)$$

For frequencies, much lower than the plasma frequency this value tends to be zero, and for frequencies above the plasma frequency the increment is $lim(\omega) \to \infty = 1$ depending on the permittivity value of the TCO. Additionally, the transmission coefficient also depends on the energy absorbed through the lossy dielectric. The transmission coefficient is given by the electromagnetic skin depth δ. The value of δ constrains the loss of energy in the electromagnetic wave when it goes through the TCO thickness t, so that, the light transmission through the TCO is approximated by equation (2.10) [19]:

$$T(t) \cong e^{\left(\frac{-2t}{\delta}\right)} \qquad (2.10)$$

Where t is the thickness of the film, and δ is the skin depth for the visible light. By recalling equations 2.6 to 2.9 we can obtain the skin depth:

$$\delta \approx \frac{2m^*\omega^2\tau}{Z_\infty q^2 N_e} \tag{2.11}$$

Where Z_∞ is $377/\sqrt{\varepsilon_\infty}$, m^* the effective mass, ω frequency at visible light, τ is the scattering/relaxation time, Ne electron density, and q the electron charge.

From these equations, we can infer that to obtain higher transmission a thinner film must be used. Moreover, according to the previous statements, the light absorption, and the energy conduction of the TCO have a duality (i.e., transparency and conductivity) that generates two different equations.

The generated equations determine the skin depth at frequencies where the TCO does not have excellent transparency, but it does have a good conduction, case (1), and case (2) where the TCO has good transmission:

(1). $\omega_p > \omega$, $\omega\tau \ll 1$

$$\varepsilon_2 \approx \frac{\omega_p^2\tau}{\omega} \gg |\varepsilon_1|, \qquad \delta \approx \left(\frac{2}{\omega\mu\sigma}\right)^{\frac{1}{2}} \tag{2.12}$$

(2). $\omega_p < \omega$, $\omega\tau \gg 1$

$$\varepsilon_2 \approx \frac{\omega_p^2\tau}{\omega^3\tau} \ll |\varepsilon_1|, \qquad \delta \approx \frac{2m^*}{Z_\infty q^2} \frac{\omega^2\tau}{N_e} \tag{2.13}$$

For these two cases, it is assumed that $\omega < \frac{E_g}{\hbar}$, $Z_\infty = \frac{377}{\sqrt{\varepsilon_\infty}}\Omega$, and $\varepsilon_1 \approx \varepsilon_\infty$. It is important to notice that when the mobility of the electrons of the material increases, it improves the conductivity as well as the transmission, the same effect happens when m^* is increased. Consequently, when choosing a TCO for antenna fabrication it is crucial to consider the free electron mass m^*, the electron

mobility μ_e and the electron density N_e, these values depend of the structure and shape of the E and K bands of the TCO as shown in Figure 2.12:
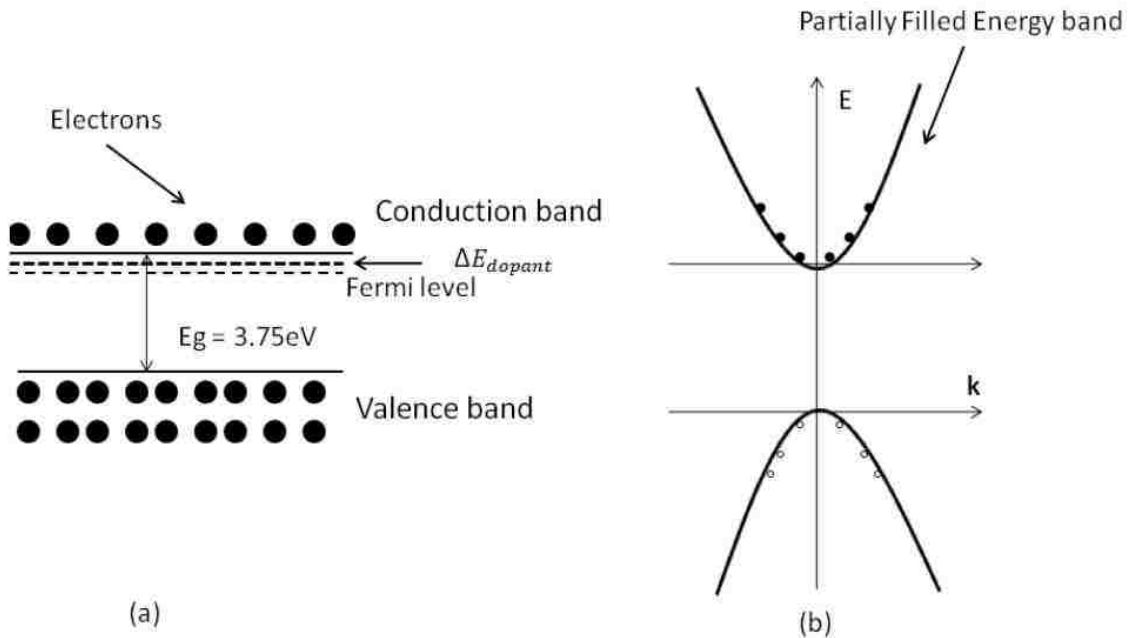
Figure 2.12 (a) TCO band diagram with doping in the conduction band, (b) doped TCO Energy band structure [2].

2.5.1. *Deposition Process*:

There are different thin film deposition methods: Thermal deposition, pulsed laser deposition, spray pyrolysis, DC sputtering, and RF sputtering. These methods can impact the oxide doping and the deposition rate. Figure 2.13 shows the power coefficient of absorption and transmittance versus thickness of the film.
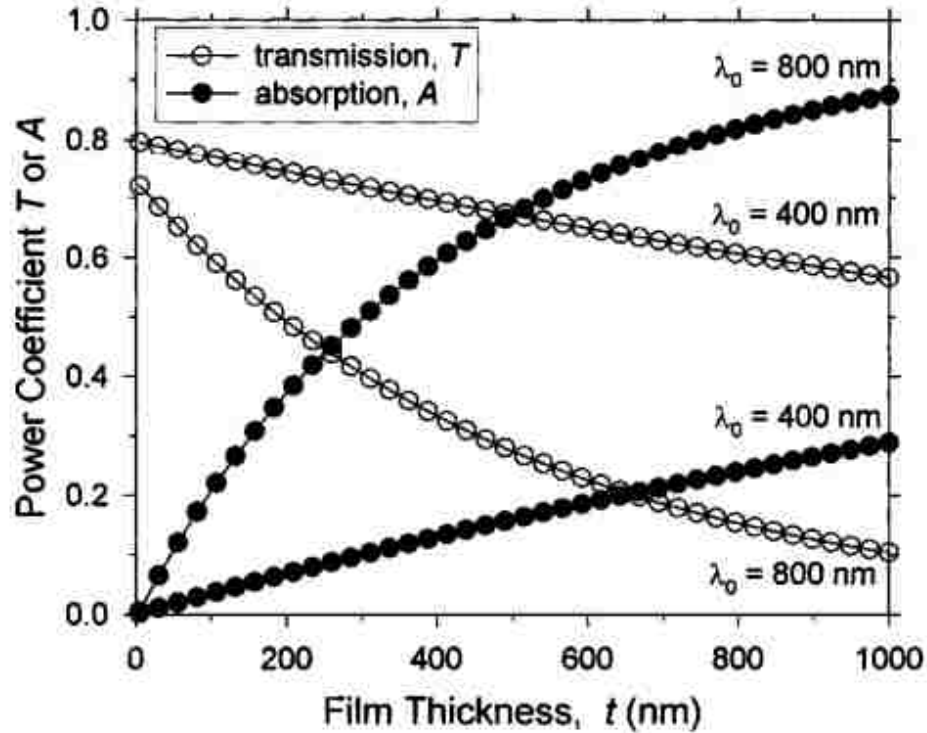
Figure 2.13 Power transmission and absorption coefficients T and A as a function of film thickness t for an ITO film of electron density [37].

The efficiency of the material is crucial when designing an OTA, and it is determined by the conductivity of the film. For TCO's the parameters that affect the conductivity depend on the doping of the material. In the case of ITO, [14], it is tin oxide doped with indium, the plasma frequency must be lower than the visible wavelength to be efficient. Moreover, a TCO is conductive if its operational frequency is smaller than the plasma frequency of the material. The surface resistance can be obtained from equation (2.14) and the electrical conductivity can be obtained as its inverse:

$$Rs = \frac{1}{(N_e q \mu_e t)} \tag{2.14}$$

Since the thickness t needs to be greater than the skin depth, then a higher conductivity requires a thicker film with higher N_e and μ_e. Although for high transparency thinner films are required, both transparency and conductivity should be maximized. For instance, to maximize optical transparency and electrical conductivity on ITO films, the electron density N_e must be at its maximum: $Ne = 1.5 \times 10^{21} cm^{-3}$, and electron mobility must reach its maximum value. From the actual technology in materials, high quality ITO films have been found to have an electron mobility of $\mu_e = 50 cm^2 V^{-1} s^{-1}$ [14].

In [14], electron density N_e, the electron mobility μ_e, the thickness, the transparency, and the efficiency for antennas designed at 2.5GHz were studied and correlated. It was shown that the antennas with higher efficiency are the ones with higher electron mobility.

The operating frequency of the antenna is also critical in determining the skin depth of the film. Since at higher frequencies the skin depth is smaller, more efficient antennas can be designed. For ITO films, the antennas are more efficient at frequencies greater than 5GHz making the material feasible for integration with solar panels.

Optically transparent antennas can also be designed and fabricated with meshed conductors. The fabrication of such antennas is easy, and they are efficient due to the high conductivity of the metal. However, the manufacturing process of meshed antennas becomes difficult at higher frequencies, the reduction of the antenna size is a critical point.

The emphasis of this dissertation is the design, optimization, and fabrication of transparent antennas using TCOs based on AZO. The various advantages of this material, including efficiency, cost, the environmentally friendly fabrication, and their ease of integration with photovoltaics are presented and analyzed in details.

Chapter 3: Why Aluminum Zinc Oxide?

This section presents the fabrication and optimization process for TCO films based on Aluminum Zinc Oxide AZO. The characterization of the films was performed for both DC and RF in order to establish the AZO behavior for integration with photovoltaics, and their feasibility for RF devices such as OTAs.

Since zinc oxide ZnO, doped with aluminum Al: ZnO, or AZO, has demonstrated to have good electrical conductivity properties, as well as, high transmittance in the visible region, it was chosen as a good candidate for integration with photovoltaics in our research problem. Although the material has not been reported for antenna fabrication, AZO films have been studied for integration with photovoltaics as top contacts [38]. Yet, these studies did not include RF devices, which is the focus of this dissertation. For integration with photovoltaics, a TCO must have low sheet resistance Rs, lower than 10 Ω/square, and high optical transmittance $Topt$ higher than 80%.

Desired properties for AZO films can be obtained when optimized during the sputtering process by controlling the power and gas concentrations; and during the annealing process by controlling annealing time and reaching temperatures higher than 200°C [38]. Moreover, a complete optimization process must include measurements of the films to avoid efficiency degradation. Measurements such as surface roughness avoid light trapping defects by assuring a smooth-uniform film; and measurements for UV-Vis transmittance and absorbance warantee a high transmittance level of the film.

3.1. *Optimization Process*

The work presented here outlines an optimization process for AZO films for Optically Transparent Antennas OTAs that is usually adopted for integration as the top contact on photovoltaics. These OTAs can be used for energy harvesting and communications antennas in a small satellite platform.

3.1.1. *Deposition Process*

In this process, the AZO film was prepared by sputtering thin layers of zinc oxide and aluminum on silicon wafers. The sputtering process was done by using the thin film deposition system *PVD 75 Kurt J Lesker* at the Center for Integrated Nano Technologies (CINT) operating at 13.7 MHz. It was not used as multitarget deposition but single target deposition process in order to keep the purity and to control the power and rate deposition of each target. Figure 3.1 shows the deposition process carried out at CINT.
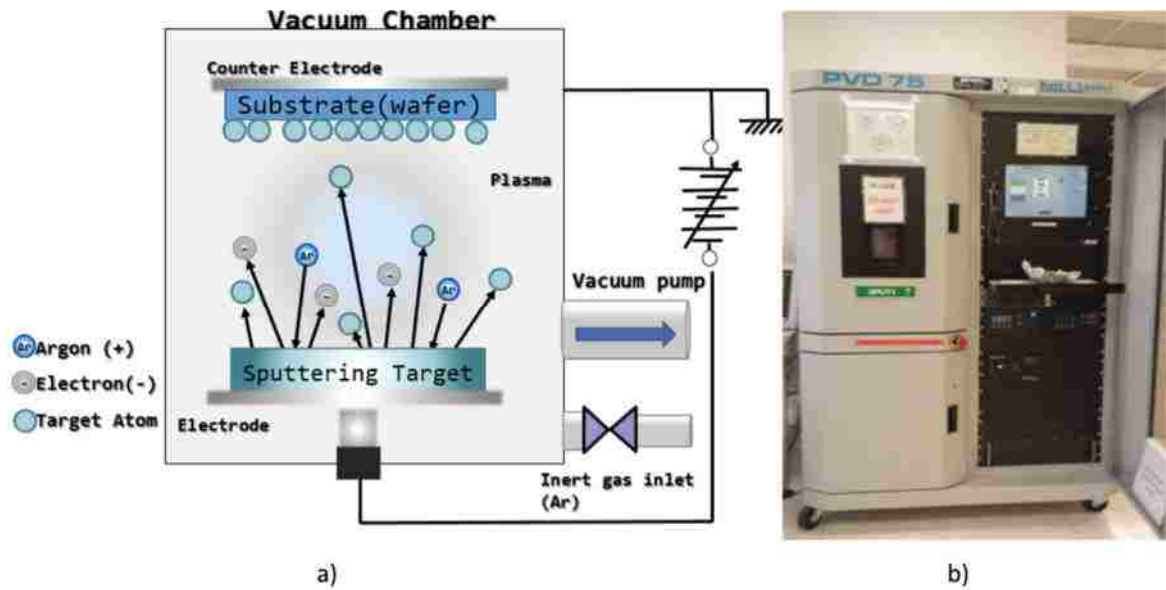
Figure 3.1 a) Deposition process, and b) sputtering machine.

The typical pressure, prior to the deposition of the Al and the ZnO, was $2.0 \times 10^{-6} mbar$ with a typical power of 110 W for Al, and 150 W for ZnO. Argon Ar gas was introduced in the chamber with a partial pressure of $8.0 \times 10^{-3} mbar$. In order to control the material thicknesses, different deposition rates were used to determine the distinctive rate for each material. To establish an optimal deposition rate, different depositions of ZnO and Al were done on a silicon wafer, and these samples were later measured and compared. The optimal deposition rate for ZnO was obtained to be $\mathbf{1.594}\, nm/min$, and for Al was $0.4915\, nm/min$. Here a total of four layers of the composite Al and ZnO were deposited with each layer having a thickness of 5nm for ZnO, and 1nm for Al. The total thickness of one sample was 24nm. Figure 3.2 shows the deposition scheme for these layers. A number of samples were taken after deposition, and the roughness of the

surface of each sample was measured in the search for the most uniform surface. By achieving a uniform surface, the light trapping defects were minimized.
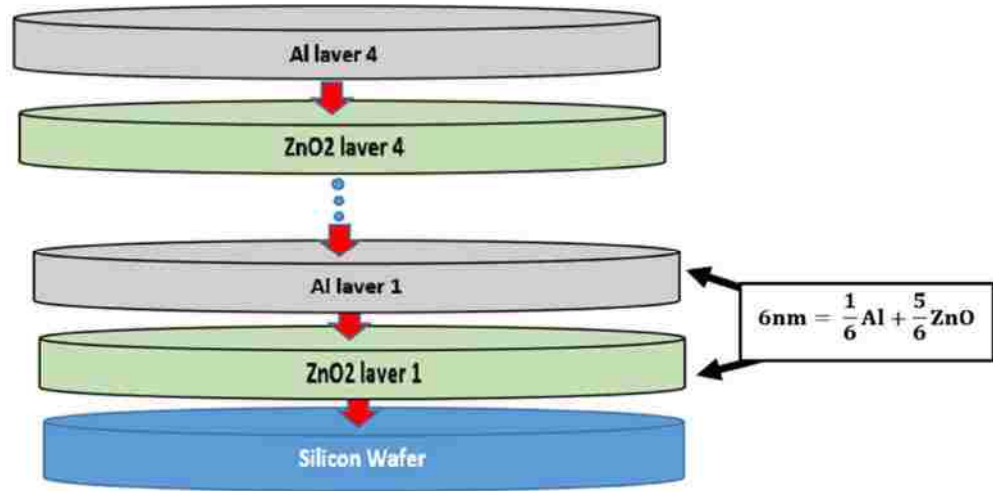
Figure 3.2 Scheme of the deposition for Al and ZnO layers [39].

3.1.2. *Annealing*

The conductivity of a TCO is enhanced by increasing the mobility of the electrons. This mobility can be altered by controlling the carrier concentrations on the doping through the gas concentrations during sputtering, or by annealing the films at high temperatures. In the annealing process, the diffusion of the materials is triggered, and the layers of ZnO are doped by the layers of Al.

In order to establish the ideal fabrication procedure for AZO films, four different samples were annealed using a horizontal furnace, with a constant

nitrogen gas flowing. Two of the samples were heated at 350°C for 24 and 48 hours, and other two were heated at 450°C for 24 and 48 hours.

3.2.   *Electrical Characterization*

After annealing, the sheet resistivity of the samples was measured using the four probe technique.   In this method, a current was passed by the two outer probes and the voltage was measured through the remaining two inner probes. The four probe measurement setup is shown in Figure 3.3.
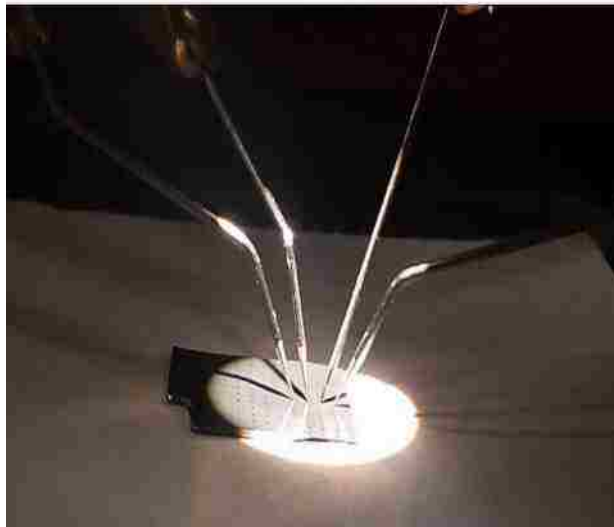
Figure 3.3 Four probe setup measurement.

Table 3.1 shows a comparison of the DC conductivity as a function of the annealing temperature and the annealing time. The lowest resistivity was $6.85\times10^{-6}\Omega*cm$ corresponding to the sample annealed during 48 hours at 450°C. The DC conductivity for this sample was obtained to be $3.48\times10^5\,S/cm$.

Table 3.1 Annealing temperature and times compared with resistivity and DC conductivity.

Annealing ºC	Time	Bulk Resistivity Ω*cm	DC Conductivity σ/cm
350	24	2.46E-04	4.50E+03
	48	1.67E-04	1.14E+04
450	24	1.28E-05	2.50E+05
	48	6.85E-06	3.48E+05

With the end of determine how much ultraviolet-visible light (UV-Vis) is being absorbed, and transmitted by the AZO films, the material was measured by spectroscopic ellipsometry. This method measures the change in light polarization and finds the changes in amplitude and phase when the light is directed to the sample. When these changes of light polarization are known, the optical properties of the material can be determined.

When a light beam with a power P_o impignes a material, part of its power is absorbed while part of it is transmitted with a power P, hence the percentage of transmittance can be calculated by equation 3.1 [40]:

$$\%T = P/P_0 \cdot 100 \qquad (3.1)$$

The absorbance can be calculated in different ways having the transmittance in (3.1) as follows [40] :

$$A = \log_{10} {P_0}/{P} \tag{3.2a}$$
$$A = \log_{10} {1}/{T} \tag{3.2b}$$
$$A = \log_{10} {100}/{\%T} \tag{3.2c}$$
$$A = 2 - \log_{10} \%T \tag{3.2d}$$

The relationship between absorbance and transmittance is shown in equation 3.2 and Figure 3.4. According to this, if there is no absorption in the material, the percentage of transmittance is 100%. On the contrary, if the light is all absorbed, the absorption is infinite and the percentage of transmittance is zero as shown in Figure 3.4.
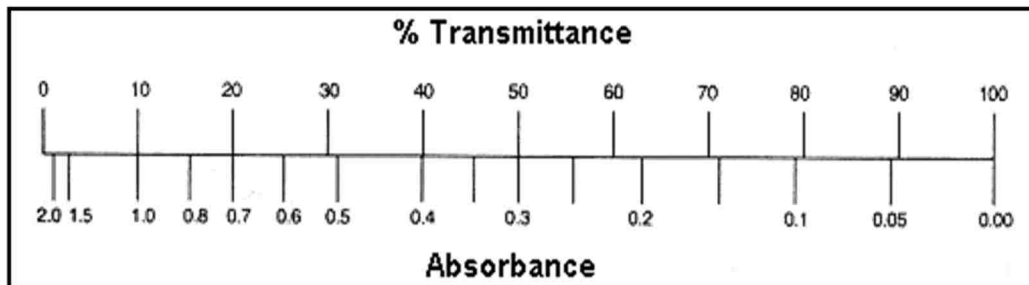
Figure 3.4 Transmittance-absorbance relationship [40].

The measured absorption coefficient is presented in Figure 3.5. Figure 3.5 shows that the lowest absorption coefficient, in the order of 0.07, vs. the U-Vis region is associated to the sample annealed for 48 hours at 450°C. From the absorbance coefficient, the transmittance of the samples was determined using equation *3.2d*, and it is depicted in Figure 3.6. By using the values of the sample

47

with the lowest absorbance it was found the maximum transmittance value to be

close to 86%:
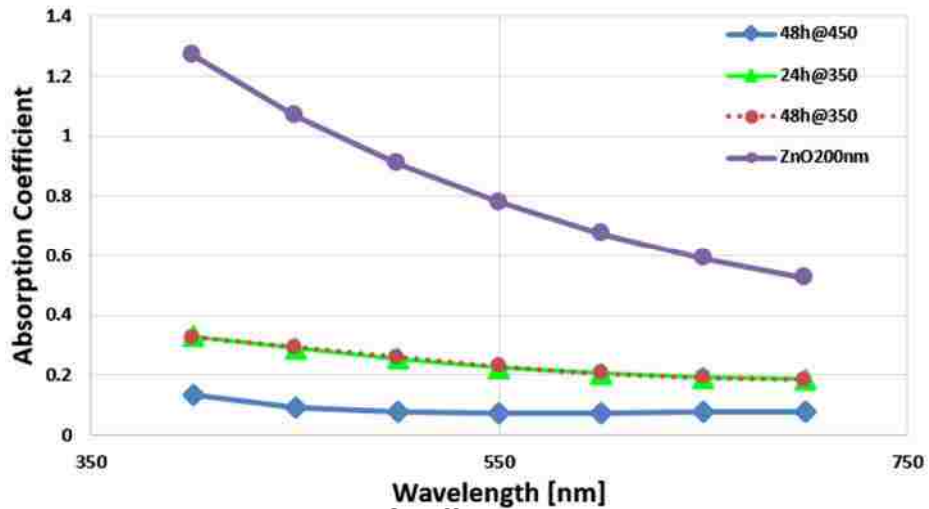
Figure 3.5 Measured Absorption Coefficient vs. UV-Vis wavelength.
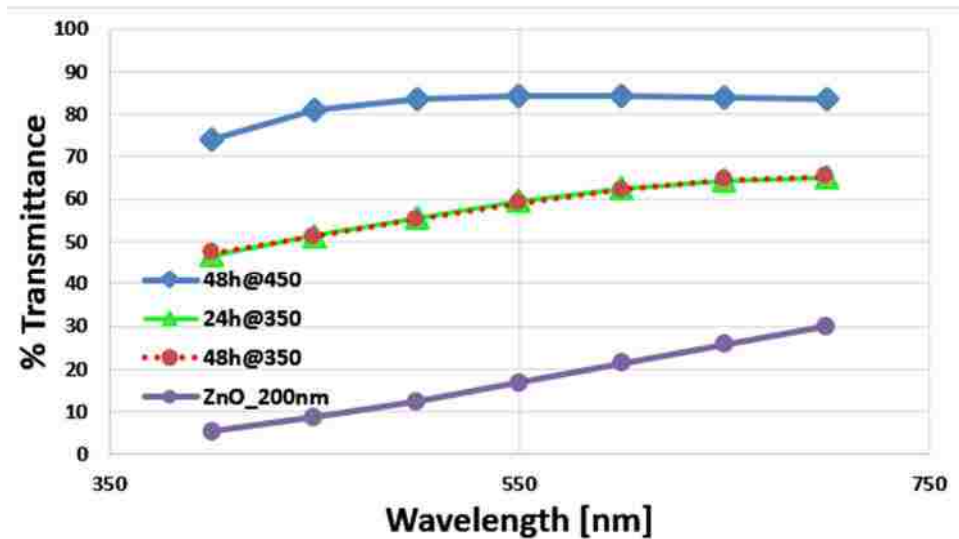
Figure 3.6 Percentage of transmission for AZO samples vs. UV-Vis wavelength.

Figures 3.5 and 3.6 show the results for the AZO annealed samples

compared with an annealed sample of ZnO without the Al doping. This

comparison was useful to determine the effect of the aluminum doping into the

zinc oxide. In fact, the aluminum doping does enhance the TCO transmittance in the visible region.

3.3.   *RF Characterization*

The four probe method, explained in section 3.1.3, and shown in Figure 3.3, is only useful when characterizing the electrical DC properties of the material. In order to characterize the samples for a broad range of radio frequencies, it is necessary to employ a different method. Some methods have been used for this matter. In [41] the author describes a method of measuring the surface losses of superconductors samples. In his method, the author employs the quality factor Q to obtain the conductivity. The results of this method have a high level of accuracy but these measurements require a small bandwidth which makes this approach not suitable for wideband RF characterization.

Another method is to employ the transmission, and the reflection coefficients [Tx/Rx] to extract the conductivity. In the literature some researchers employed the [Tx/Rx] method to obtain the complex permittivity and the conductivity for different types of samples, [42] [43]. One technique that has been used to do the transmission and reflection measurements is through an open-ended coaxial probe [44].

This dissertation makes use of the [Tx/Rx] method. In this method the RF conductivity of the AZO film was extracted by measuring the coefficients for transmission and reflection through an open-ended coaxial probe. The probe was

connected to the Vector Network Analyzer (VNA) PNA-X N5247A. To perform these measurements, five different thicknesses of the AZO material were deposited onto five different thick glass substrates with 5mm of thickness, and 1in wide by 2in length as total dimensions. The thicknesses of the AZO films were chosen to be 12nm, 24nm, 48 nm, 72 nm, and 96nm to establish the effect of thickness on RF conductivity and on optical transparency. The measured parameter was the S11 (return loss) for each sample, and the conductivity was extracted by employing the mathematical process detailed in the next few paragraphs (matlab code in Appendix B).

The first round of measurements was done with the five non-annealed samples with five different thicknesses; and it was followed by measurements taken on the same five different samples, but after annealing them during 48 hours at 450°C. By measuring non-annealed and annealed samples it was possible to compare the changes on the RF conductivity before and after annealing. The setup for the measurements is shown in Figure 3.7, C-clamps were used to assure the contact between the RF probe and the sample.
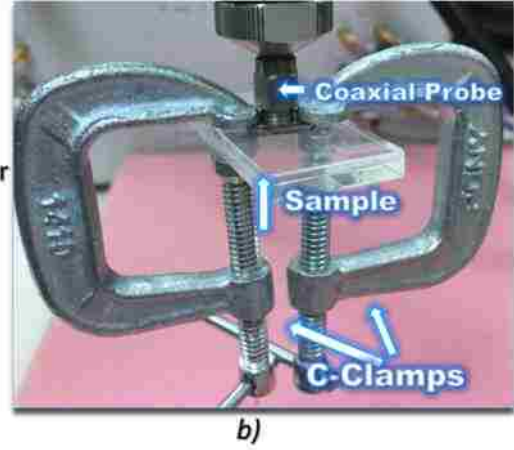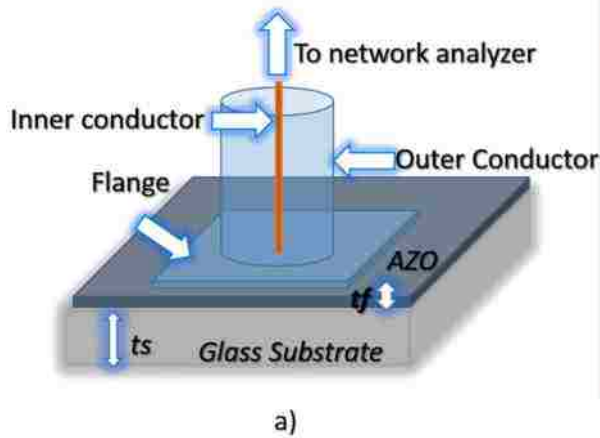
Figure 3.7 Measurement setup for RF characterization a) Glass Substrate schematic, and b) Picture of the glass substrate with C-clamps and coaxial probe.

Before measuring the samples, it was necessary to calibrate the coaxial probe [45]. The flow diagram shown in Figure 3.8 represents the coaxial probe reflection and transmission:
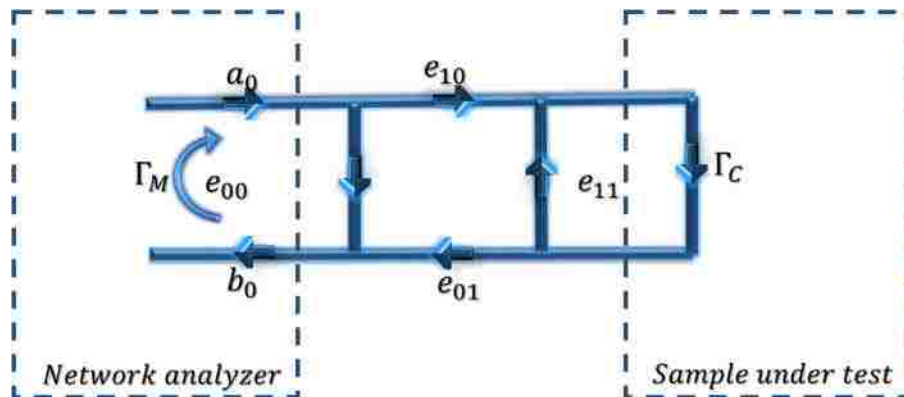
Figure 3.8 Flow diagram of the signal showing the incident and reflected waves.

In the signal flow diagram e_{00} is the directivity error while e_{01} and e_{10} represent the reflection tracking error, finally, e_{11} is the source matching error. When solving the diagram, the measured reflection coefficient Γ_M, and the calculated reflection coefficient Γ_C are [45]:

$$\Gamma_M = \frac{b_0}{a_0} = e_{00} + \frac{e_{01}e_{10}\Gamma_C}{1 - e_{11}\Gamma_C} \tag{3.3}$$

$$\Gamma_C = \frac{\Gamma_M - b}{-c\Gamma_M + a} \tag{3.4}$$

Where $a = e_{01}e_{10} - e_{00}e_{11}$

$b = e_{00}$

$c = -e_{11}$

Then, three calibration measurements (open, short and load) were performed to find a, b, and c by using equation (3.5) where the subscript i represents either open, short or load [45]:

$$a\Gamma_{C,i} + b - c\Gamma_{C,i}\Gamma_{M,i} = \Gamma_{M,i} \tag{3.5}$$

Once the calculated gamma Γ_C was found, the RF conductivity was extracted by using the thin film approximation in [44]. In order to calculate the impedance of the substrate together with the thin film Zt, equation (3.6) was used, in the equation Zc refers to the characteristic impedance of the coaxial cable given by equation (3.7):

$$Z_T^{eff} = Zc \frac{1 + S_{11}}{1 - S_{11}} \tag{3.6}$$

$$Zc = Z_0 \frac{\ln(b/a)}{2\pi\sqrt{\varepsilon_r}} \tag{3.7}$$

When (3.7) is replaced into (3.6) it gives:

$$Z_T^{eff} = Z_0 \frac{\ln(b/a)}{2\pi\sqrt{\varepsilon_r}} \frac{1 + S_{11}}{1 - S_{11}} \tag{3.8}$$

By employing transmission line theory (3.8) becomes [44]

$$Z_T^{eff} = Z_0 \frac{\ln(b/a)}{2\pi\sqrt{\varepsilon_r}} Z_f^\infty \frac{Z_s^{eff} + Z_f^\infty \tanh(jk_f t_f)}{Z_f^\infty + Z_s^{eff} \tanh(jk_f t_f)} \tag{3.9}$$

By recalling Figure 3.7 a) t_f is the thickness of the film, k_f is the wave propagation constant of the film, Z_f^∞ is the bulk impedance of the film, and Z_s^{eff} is the effective impedance toward the glass substrate. The thin film approximation in [44] says that if $|k_f t_f| \ll 1$, and $Z_s^{eff} \gg Z_f^\infty$ then (3.9) can be simplified to:

$$Z_T^{eff} = \frac{\ln(b/a)}{2\pi} \frac{Z_f^\infty}{jk_f t_f} \tag{3.10}$$

The equations for the bulk impedance of the film Z_f^∞, and the wave propagation constant of the film k_f are given in (3.11), and (3.12):

$$Z_f^\infty = \sqrt{\frac{\mu_0}{\varepsilon_f' - j\sigma/\omega}} \tag{3.11}$$

$$k_f = \sqrt{\mu_0\left(\varepsilon_f' - j\sigma/\omega\right)} \tag{3.12}$$

An expression for Z_T^{eff} is obtained by substituting (3.11), (3.12) into (3.10):

$$Z_T^{eff} = \frac{\ln(b/a)}{2\pi} \frac{1}{j\omega t_f\left(\varepsilon_f' - j\sigma/\omega\right)} \tag{3.13}$$

With these equations, the conductivity can be expressed in terms of the reflection coefficient, S11, or for this case the calculated after calibration reflection coefficient Γ_C:

$$\sigma_{(\omega)} = \left(\frac{1}{t_f Z_0}\right) Re\left\{\sqrt{\epsilon_r}\frac{1-\Gamma_C}{1+\Gamma_C}\right\} [S/cm] \tag{3.14}$$

Where t_f is the thickness of the film, ϵ_r is the coaxial probe dielectric constant of the filling, and the values for $\epsilon_0 = 8.85418782 \times 10^{-12}$ m^{-3}kg^{-1} s^4 A^2 and $Z_0 \approx 377\Omega$ are the free space values.

Table 3.2 shows the maximum and the average values of the measured samples for different thicknesses, annealed and non-annealed. According with these results we can conclude that the conductivity increases when the sample is annealed, as expected. Moreover, looking at the average values for the annealed samples, we can see that the values are more uniform compared with the non-annealed samples.

Table 3.2 AZO RF characterization values all values are σ [S/cm].

tf	σ-12nm	σ-24nm	σ-48nm	σ-72nm	σ-96nm	All_Samples-σ
Max_Non-annealed	1.316E+06	3.734E+06	2.905E+06	9.126E+05	1.383E+06	3.734E+06
Max_Annealed	7.288E+06	1.048E+07	9.974E+06	1.379E+07	1.729E+07	1.729E+07
Average_Non-annealed	3.123E+05	1.633E+05	7.533E+04	5.236E+04	4.047E+04	1.423E+05
Average_Annealed	3.385E+05	3.987E+05	3.918E+05	3.759E+05	3.768E+05	3.764E+05

For the case of the non-annealed samples, the maximum conductivity was for the sample of thickness $tf = 24\,nm$ with a conductivity of $\sigma = 3.73 \times 10^6 [S/cm]$. Whereas, for the annealed samples, the maximum conductivity was for the sample of thickness $tf = 96\,nm$, with a value of $\sigma = 1.73 \times 10^7 [S/cm]$ as expected, and according with section 2.5.1. the thicker the sample the more conductivity. Additionally, this is due to the improvement of electron mobility after annealing.

Figure 3.9 shows the comparison between the maximum RF conductivity values reached before and after annealing versus the sample thickness. The plot shows an increment on the conductivity according to the thickness, and especially after annealing. The existing direct relation of the thickness with the conductivity was explained in section 2.5.1 of this document. The thickness of a efficient conductive material should be greater that the skin depth, hence thicker film leads to higher conductivity with higher electron density and higher electron

mobility. This explains why the annealed samples have better conductivity, because their mobility is enhanced with the annealing process.
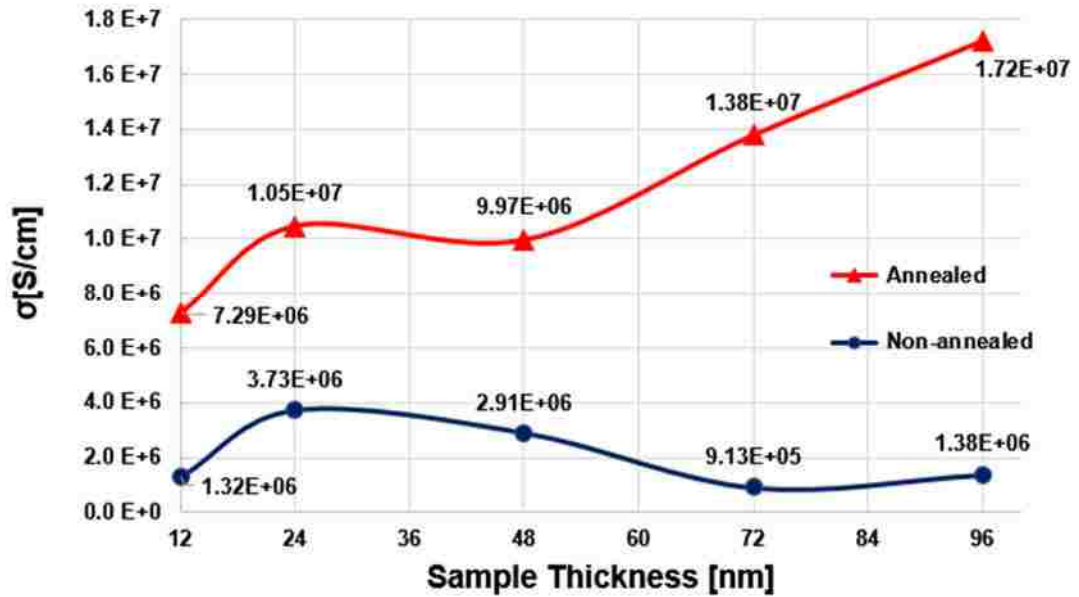
Figure 3.9 Maximum conductivities versus sample thickness.

As stated before, the maximum value of the RF conductivity was obtained for the thickest sample $tf = 96nm$, but its percentage of transparency decreased, as shown in Figure 3.10. The Figure 3.10 depicts the percentage of transmittance vs. the UV-Vis wavelength. The maximum percentage was for the sample of $tf = 12nm$ which conversely has the lowest RF conductivity (see Figure 3.9). Figure 3.11 shows the absorption coefficient vs. UV-Vis wavelength. According to Figures 3.10 and 3.11, the sample with less absorbance has higher transmittance and vice versa, as anticipated. Section 3.1.3 describes the relation between transmittance and absorbance in detail.
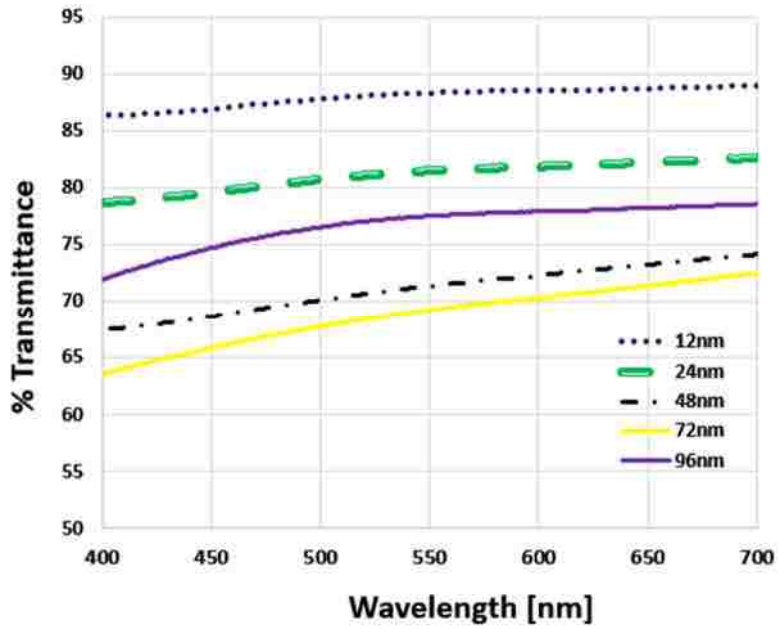
Figure 3.10 Percentage of transmittance vs. wavelength for different AZO thicknesses.
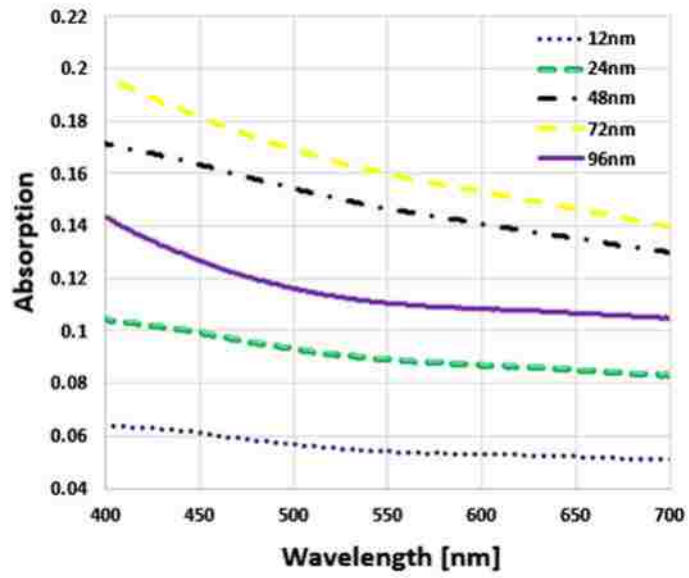
Figure 3.11 Absorption vs. UV-Vis wavelength for different AZO thicknesses.

On the other hand, the sample with maximum conductivity is the sample with a thickness of $tf = 96nm$, which has a transmittance percentage of 73% to 77%, this percentage range is acceptable but not good enough for OTA fabrication. An efficient level of transparency for transparent antennas integrated with solar cells should be at least 80%.

The optimization process of the AZO film used in this work together with the characterization (DC and RF) and transmittance/absorbance measurements, contributed to establish which characteristics must be achieved when choosing an AZO film for transparent antenna fabrication. These characteristics include: The method of deposition (gas concentration, sputtering power, partial pressure); the ideal deposition rates; the optimal annealing time and temperature; and the optimal thickness of the film with best optical properties (high transmittance and high conductivity). Furthermore, this process contributed to determine which sample was the most optimal for fabrication of OTAs for solar cell integration

After analyzing the optimization process, the characterization (DC and RF), and the transmittance/absorbance measurement results, it was determined that the sample with $tf = 24nm$ offered the best optical properties in comparison with the other four samples. The 24 nm sample possesses high transmittance, between 79% and 83%, and high conductivity $\sigma = 1.05 \times 10^7 [S/cm]$. These values make the 24nm thickness the most optimal for the applications considered in this research.

Chapter 4: Antenna Design, Fabrication Process, Experiments and Results

The foundation of this research is to find an efficient way to integrate an antenna on top of a solar panel, integration that should have the minimum effect on the light absorption by the solar panel. The optimal way to accomplish this integration is to design an Optically Transparent Antenna (OTA). Different transparent conductor materials have been used in the past to design OTAs, (see Chapter 2, section 2.4). However, the efficiency of those materials has not been optimized yet. In the search of finding the most effective way to perform this solar cell-OTA integration, new transparent conductive materials were used in the experimental section of this dissertation. This section explains, in detail, experiments with different transparent conductors; as well as OTA designs, fabrication and measurements.

A transparent material based on Silver-Tin Oxide (AgHT) coated with Polyethylene Terephthalate (PET) was the first material tested. This AgHT was chosen because of its reasonable optical transparency and its commercial availability [18].Moreover, the material can easily be attached to a solar panel.

4.1. *AgHT Experiments.*

AgHT is a silver coated transparent material commercially available in two options [25]: AgHT-4 and AgHT-8. The numbers 4 and 8 refer to the sheet

resistance of the material, meaning that AgHT-4 has $4\Omega \cdot m$ of resistance, while AgHT-8 has $8\Omega \cdot m$ [5] . The material consists of a layer of silver conductor Ag sandwiched in between two tin oxide layers, and coated with PET. Figure 4.1 shows the basic structure of the material.
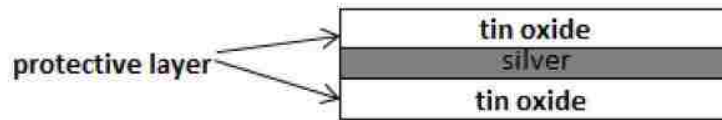
Figure 4.1 Basic structure of AgHT [5].

4.1.1. *Monopole AgHT Antenna Experiment*

The first experimental task was to test the AgHT feasibility for antenna design and fabrication. In the first experiment, the AgHT-4 was used to fabricate a monopole antenna. This AgHT had a thickness of 1.75 mm, with 40% of its thickness being PET (0.07mm), and 60% being the conductive layer (1.05mm) [46].

The design was a monopole antenna and it was simulated by means of the High Frequency Structure Simulator (HFSS). The material properties of AgHT-4 and PET were added to the existing material list in the software. The PET loss tangent delta frequency dependence is shown in Table 4.1 [5].

Table 4.1 Frequency dispersion fit for PET

Frequency [GHz]	Value
1.8	0.006479
3.9	0.005965
6.0	0.00586
8.1	0.00583
10	0.00581
12.3	0.0058
14.4	0.005791
16.5	0.005781
18.6	0.005771
20	0.005761

The designed monopole antenna was fabricated and soldered to an SMA connector by employing cold soldering instead of traditional soldering due to the AgHT and PET temperature sensitivity. The cold soldering was done by using a highly conductive silver epoxy.

The monopole was designed to resonate at 2.4GHz. The antenna has a height of 29.55mm and a width of 5mm. In Figure 4.2, the fabricated monopole, and the comparison of the measured and simulated results are shown. The AgHT fabrication process and measurement was arduous due to the need to remove the PET coating layer to reach the conductive part of the material; without removing the PET there was literally no contact between the monopole and the SMA. Moreover, the material texture, extremely flexible and temperature sensitive, made it potentially problematic to fabricate antennas with a more complex shape.
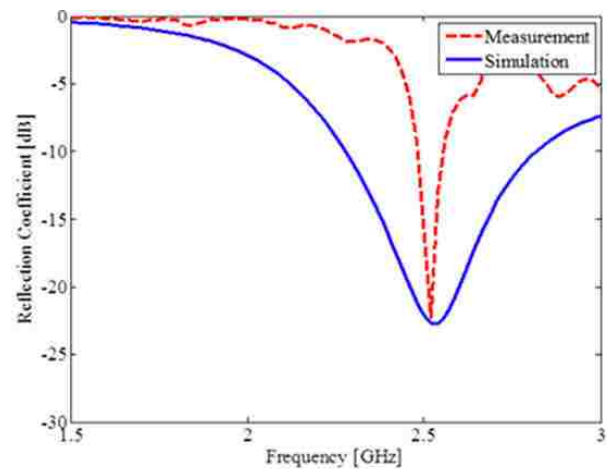
(a)   (b)

Figure 4.2 Monopole antenna in AgHT (a) fabricated prototype, (b) comparison simulated vs fabricated results.

Although the comparison shows agreement in the resonant frequency for measurement and simulation, losses presented in the material decreased the efficiency of the antenna. Thus, it was concluded that the AgHT-4 material is not very efficient and useful for antenna fabrication.

4.2. *Experiments with AZO*

Since the AgHT experiments demonstrated that this material had high losses, it was necessary to try different approaches. The starting point for the next round of experiments was to perform simulations through HFSS and the Computer Simulation Technology (CST) Microwave Studio. Firstly were simulated and analyzed the shape and the feeding mechanism of the most appropriate antenna to be implemented on a solar panel.

Since one approach for achieving efficient OTAs is to use meshed conductor materials, a bowtie antenna using meshed copper was designed and it was compared with a transparent conductive oxide TCO whose optical properties were found in the literature [28]. The dimensions of the antenna are: Arm length 61 mm, flare angle 92mm, curve 97.84; SiO2 substrate thickness 100μm, and Si substrate thickness 700μm, substrate dimensions of $152x152mm$. The meshed antenna design was done by optimizing conductive copper lines to make sure that the absorption of the solar energy by the panel was not affected. The

meshed optimal parameters arre: Optimal separation of 5 mm, and optimal thickness for the mesh lines of 0.5 mm.

It was found that by employing the TCO values in [25] the behavior of the antenna was comparable with that of a meshed conductor. In terms of gain, a TCO obtained 2.2dB, and a meshed conductor obtained 5.9dB. However, when trying to increase the frequency range, the optimization of the meshed antenna did not work, and the efficiency of the antenna decreased. Figure 4.3 shows the geometry of the bowtie antenna.

a)   b)
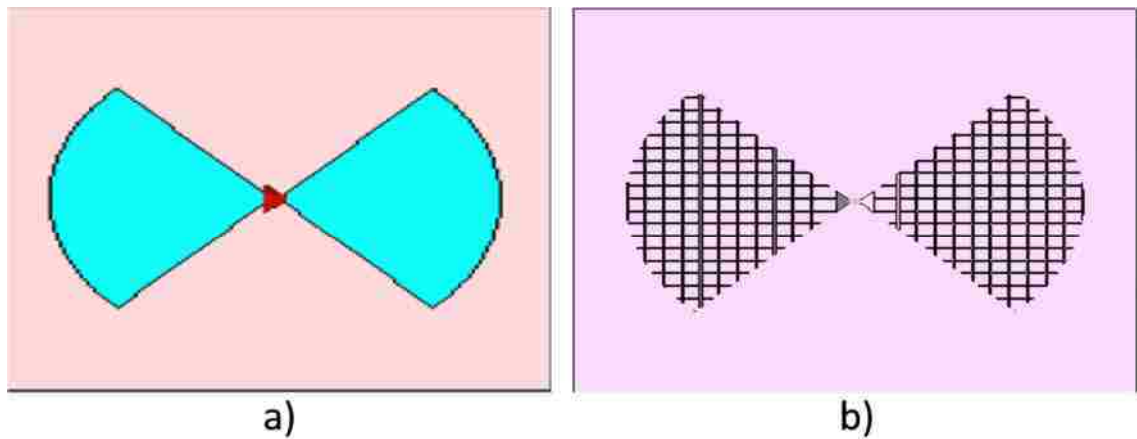
Figure 4.3 Bowtie antenna structure a) TCO, and b) meshed copper antenna.
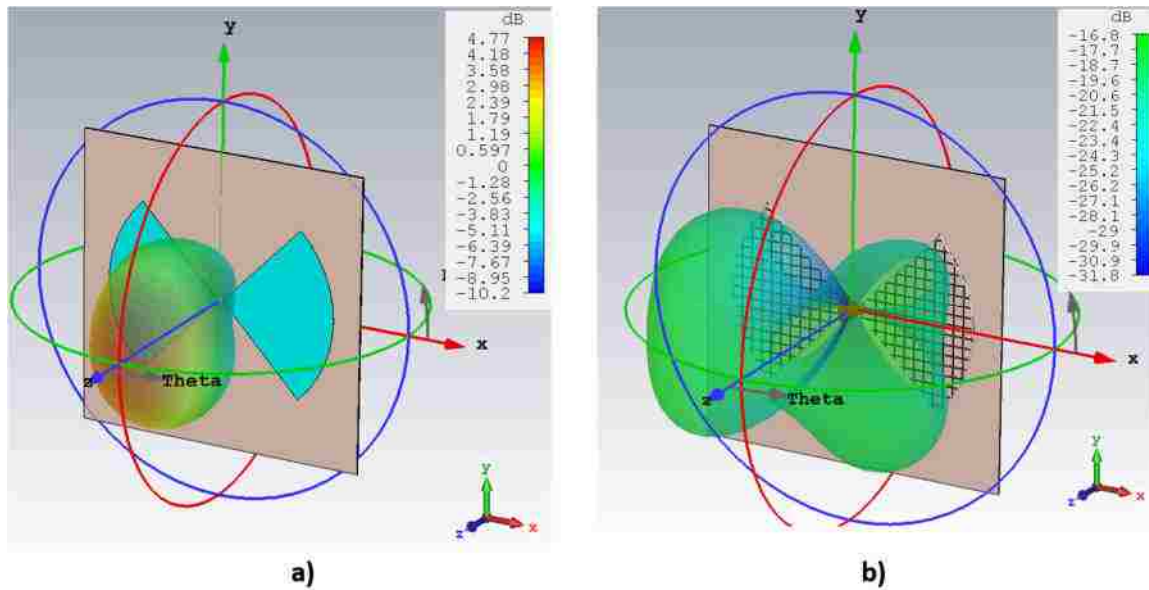
Figure 4.4 Radiation pattern and gain for bowtie antenna a) AZO film, and b) meshed conductor.

According to the simulation results shown in Figure 4.4, it was noticed that the efficiency for the meshed conductor was decreaded. , hence, it was concluded, that the best approach for integration, in this case, was to use a TCO. This kind of transparent conductor can be more useful for any antenna geometry and in any size without compromising the efficiency of the solar cell.

The TCO's advantage of having electrical conductivity at RF frequencies while still having high transmittance in the visible region motivated the use of this material for antenna designs without any geometry restrictions. Arrays with their entire feeding network can be also designed and fabricated by using TCO, thus representing a significant advantage when high gains are needed. For instance, high gain antenna arrays with entire feeding networks on TCO can be utilized for satellite communications.

The research was then focused on the TCO, and the purpose was to find the most suitable TCO for the antenna-solar cell integration. Since the most used TCO is ITO (indium tin oxide), its optical properties were investigated. Still, the high cost of the material, led to the search of a more suitable material for research with similar optical properties. According to the previous investigations, as stated in Chapter 3, the research was directed to using zinc oxide doped with aluminum, AZO. This material had similar properties and presented the advantage of being more cost efficient than ITO.

Different simulations were done with AZO in order to compare and establish its feasibility as material for optically transparent antennas integrated with solar cells. The first experiment used a wide band spiral antenna made of AZO for frequencies under 10GHz to test the material for applications supported at this range such as WLAN, GPS, UMTS and Bluetooth. This spiral antenna whose dimensions are shown in Figure 4.5, was a two-arm log spiral antenna, with angular arm width of 90 degrees, an inner diameter of 0.875mm, a number of turns of 2.3054 mm, and a total diameter of 248.976mm.

a)

b)

S-Parameters [Magnitude in dB]

Frequency / GHz

c)
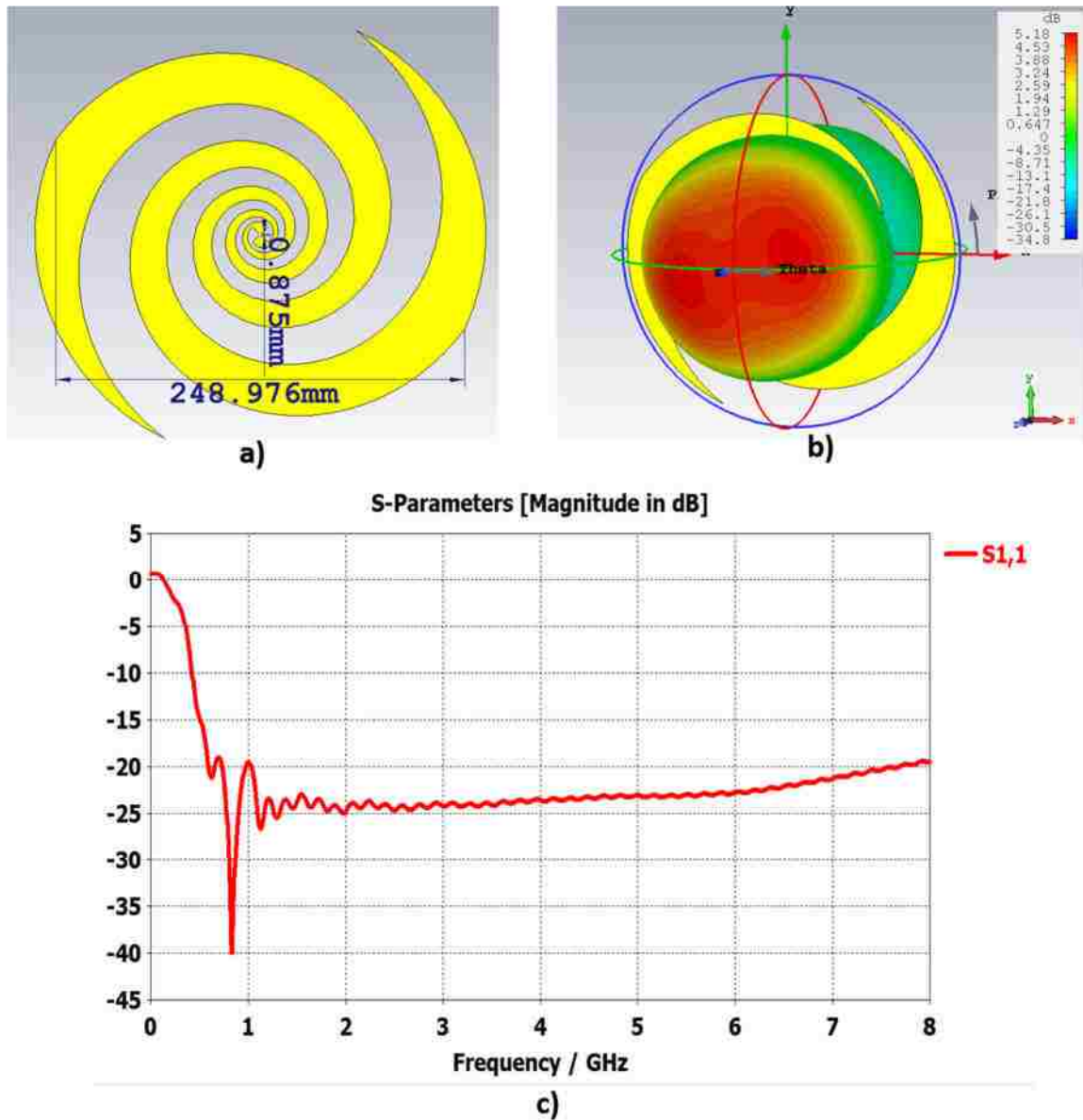
Figure 4.5 Spiral antenna copper a) structure of the antenna b) S-parameters bellow -10dB from frequencies under 10GHz, and c) gain about 5.18 dB.

In the first simulation with the spiral antenna, the AZO film was tested as conductor without any substrate and it was compared with the same spiral design simulated with copper as a conductor. Figure 4.5 shows the results for the spiral

antenna simulated with copper. The antenna had a gain of 5.18dB with a wide band behavior for frequencies under 10GHz as expected. The comparison shows that the AZO material exhibits good conducting characteristics as depicted in Figure 4.6. The antenna shows good S-parameters, and a slight decrease in gain 0.16dB being the realized gain for AZO 5.02dB. However, it does not have a negative impact in the overall antenna efficiency; hence, the material presents good characteristics for antenna design.
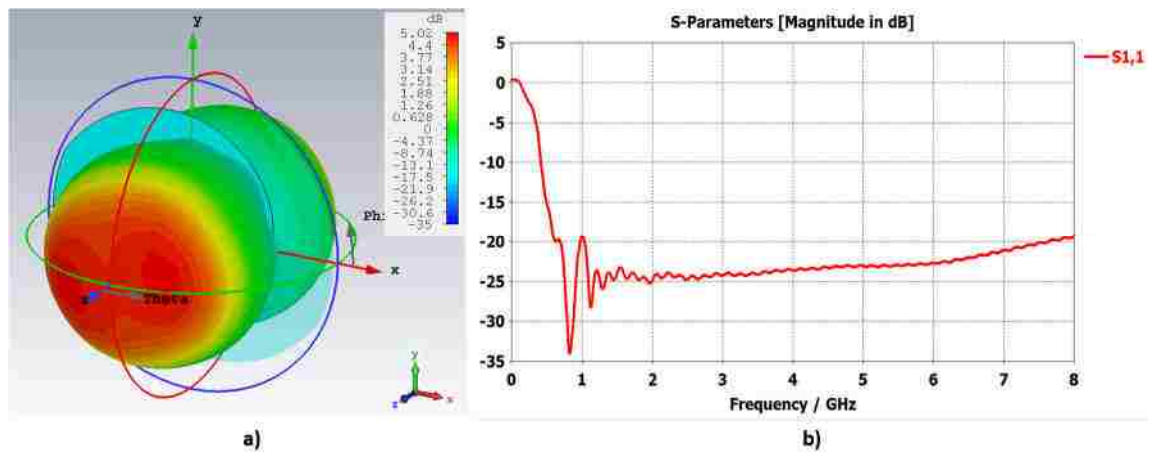
Figure 4.6 Spiral antenna AZO a) gain about 5.02dB, and b) S-parameter S11.

For the second simulation of the spiral antenna, a silicon Si substrate was added to simulate the antenna-solar cell integration. The solar cell was simulated as a silicon wafer whose parameters already exist in CST. For these simulations, the AZO optical parameters in [25] were introduced into the electromagnetic simulation software. The AZO was located over a layer of silicon dioxide SiO2, whose function was to protect and to isolate the antenna and the silicon wafer. Figure 4.7 shows the layers structure for these simulations. The silicon Si layer

had a thickness of 0.37 mm and the silicon dioxide SiO layer had a thickness of 0.1mm, while the AZO had a thickness of 0.1mm.
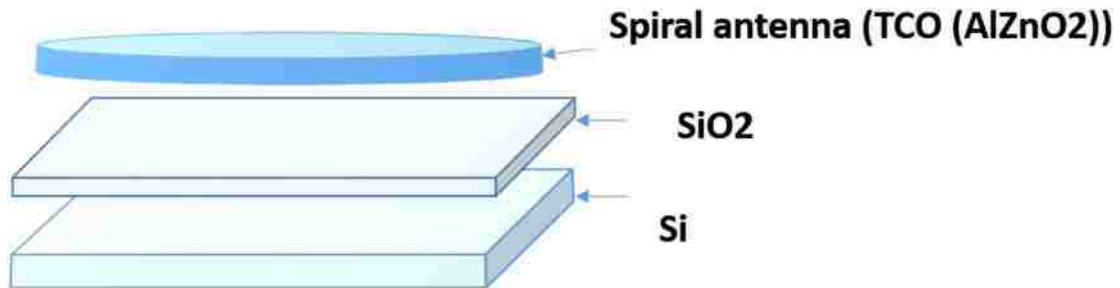
Figure 4.7 Structure AZO on top of silicon for simulations.

The simulations of the antenna on top of a SiO layer isolating the antenna from the silicon substrate still possessed a good behavior. Figure 4.8 shows that the S-parameters were under the -10dB from frequencies between 0.8GHz and 6.5 GHz approximately which is appropriate for applications under 10GHz. In the Figure 4.8, it is evident that the gain reached 4.86dB, this slight reduction was because of the high permittivity of the substrate $\varepsilon_r = 11.9$. Yet, the AZO behavior was still suitable for antenna fabrication.
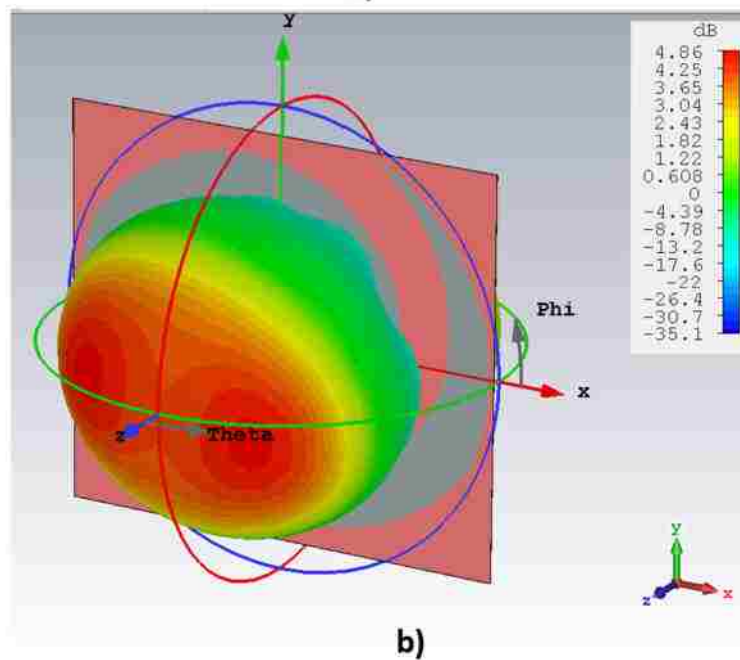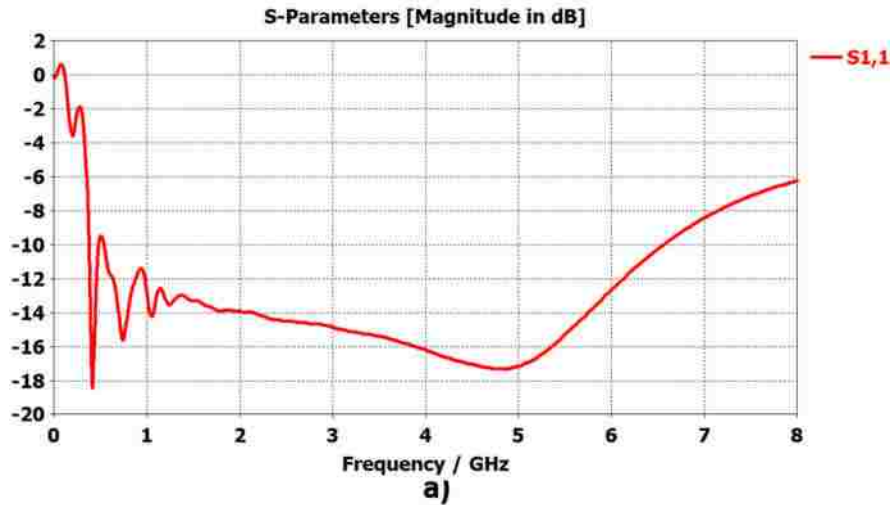
Figure 4.8 Simulation results a) the return loss, and b) the realized gain 4.86 dB.

Since there is a potential increase in the OTA's efficiency when using a superstrate [36], a simulation was done to test a superstrate layer of SiO2 on top of the AZO layer. However, the effect of this SiO2 layer did not increase the gain of the OTA. In fact, the gain decreased slightly compared with the case shown in

Figure 4.8 by 0.1dB. This is shown in Figure 4.9b. In this case, the SiO layer was located on top of the antenna to protect it, giving a newly realized gain of 4.76dB. Hence, it was concluded to not use superstrate SiO2 for antenna fabrication with AZO films.
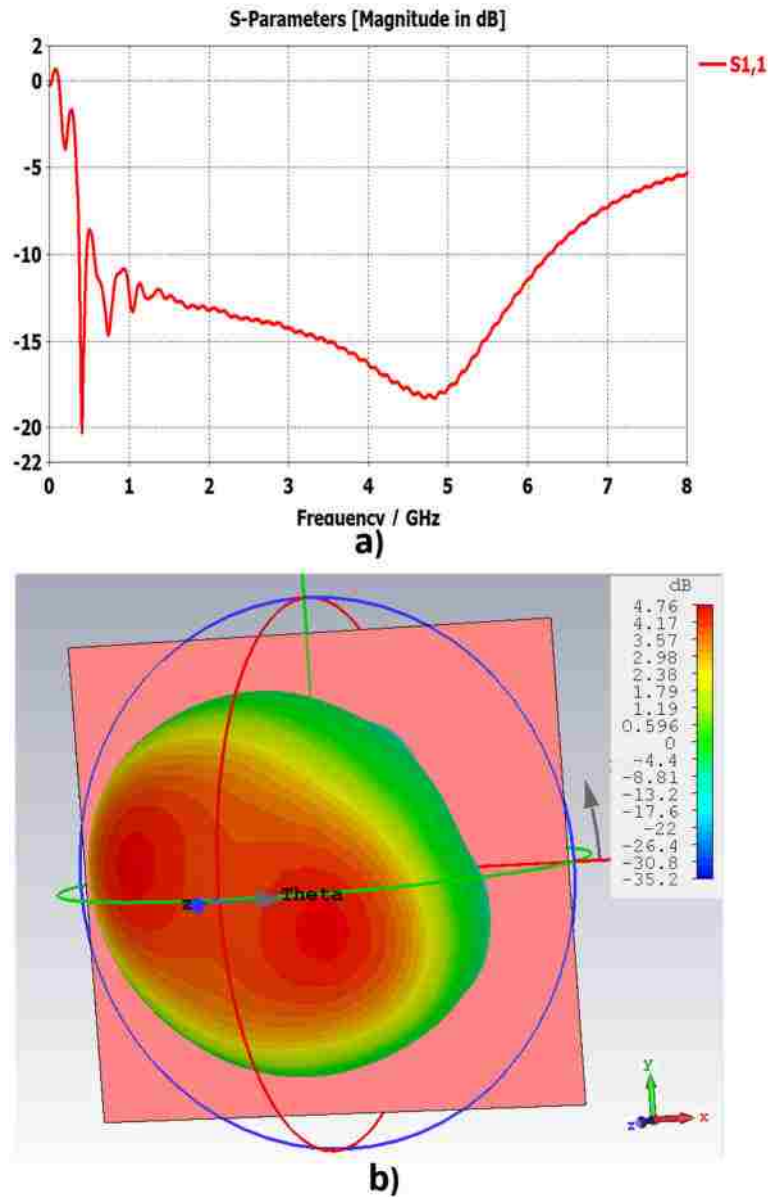
Figure 4.9 Simulation results for antenna with SiO on top a) S-parameters and b) realized gain 4.76 dB.

The AZO films optimization process results described in Chapter 3 were used for achieving the optimal parameters of high conductivity, and high transmittance. After the samples were optimized, and the characterizations (DC and RF) were done, the DC conductivity was found to be $3.4.8 \times 10^5 \, S/cm$, and the RF conductivity reached a maximum of $1.05 \times 10^7 \, S/cm$ for the sample of 24nm thickness. The optimized sample of the AZO film reached good RF conductivity and high transmittance levels, between 79% to 83%, which confirmed that the material was suitable for designing efficient optically transparent antennas able to be integrated with solar panels.

4.2.1. *Rectangular Patch Antenna*

As a proof of concept, an inset fed patch antenna was designed, simulated and fabricated with AZO film. The film was deposited on top of a silicon wafer with thickness $t = 0.37mm$ employing the optimization process described in section 3.1.

The proposed antenna was a rectangular inset fed patch antenna operating at 2.2GHz with total dimensions $17 \, mm \, x \, 26.6mm$. The antenna has a full ground plane and silicon as substrate, this substrate has the same characteristics of solar cell material; hence, the simulation was considering the effect of the AZO material on silicon solar cells.

The antenna was simulated by means of CST, the simulation was done by employing the AZO conductivity value found in the optimization process in

Chapter 3, and it was compared with a simulation done by employing a Perfect Electric Conductor (PEC). The results of this comparison are shown in Figure 4.10. The optimized AZO film exhibits good behavior with a gain of 2.78dB, as shown in Figure 4.10 a. When AZO is compared with PEC, it experiments a decrease in gain of 2.29dB; the reason for this decrease in gain is because the AZO conductivity is less than the one of a perfect conductor: AZO in average was found to have a conductivity of $\sigma = 3.98 \times 10^5 [S/cm]$, (see Chapter 3), Still, the resulting gain from the AZO material indicates that this specific ITO is suitable for designing and fabrication of efficient OTAs.
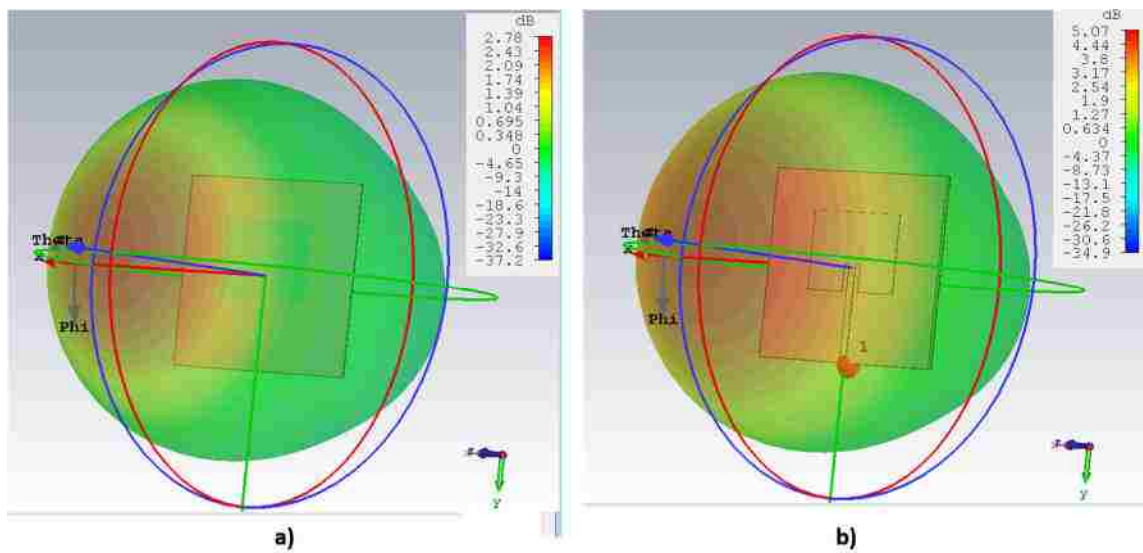
Figure 4.10 Radiation Pattern 3D and gain of rectangular inset-fed patch antenna a) AZO and b) PEC.

The design of this rectangular antenna was optimized with the goal of obtaining as much gain as possible. The dimensions of the antenna are shown in Figure 4.11 a. The total width of the patch is 26.63mm, the length is 19.41mm, with an inset feed spacing of 1.47mm, and a feeding line width of 1.91mm. Figure 4.11 b shows the return loss obtained from this structure. It is evident that the antenna has a good return loss for the designed frequency. The next step was to fabricate and perform testing on the fabricated prototype. The next section explains in detail the fabrication process and testing of the rectangular patch antenna.
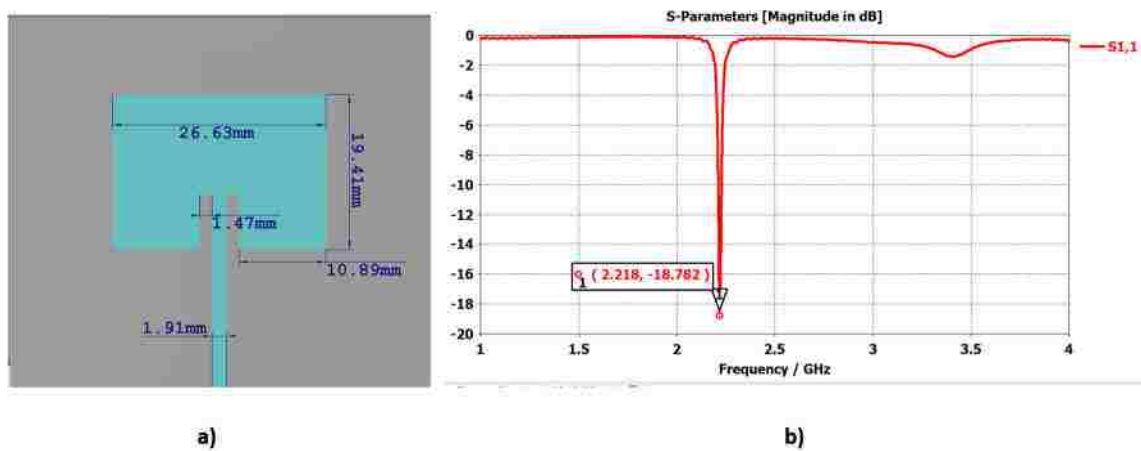
Figure 4.11 a) Structure of the AZO rectangular patch antenna with dimensions, b) return Loss.

4.2.1.1.   *Rectangular Patch Antenna Fabrication and Measurements*

The antenna fabrication process relied on photolithography processing. A mask was required to perform the processing. In this case, the Center for

Integrated Nanotechnologies (CINT) was used to generate the required mask for photolithography. The simulated design was exported to a Drawing Exchange Format (DXF) file and all dimensions were specified as shown in Figure 4.12 (left). The generated mask is shown in Figure 4.12. The mask consists of a 100nm layer of Chromium (Cr) deposited on glass plate. To write the mask on the plate, the Heidelberg Direct Write (DW) high-resolution instrument was used to generate the pattern for Cr mask plates. The entire process for designing, writing, and obtaining the mask takes about 4 weeks.
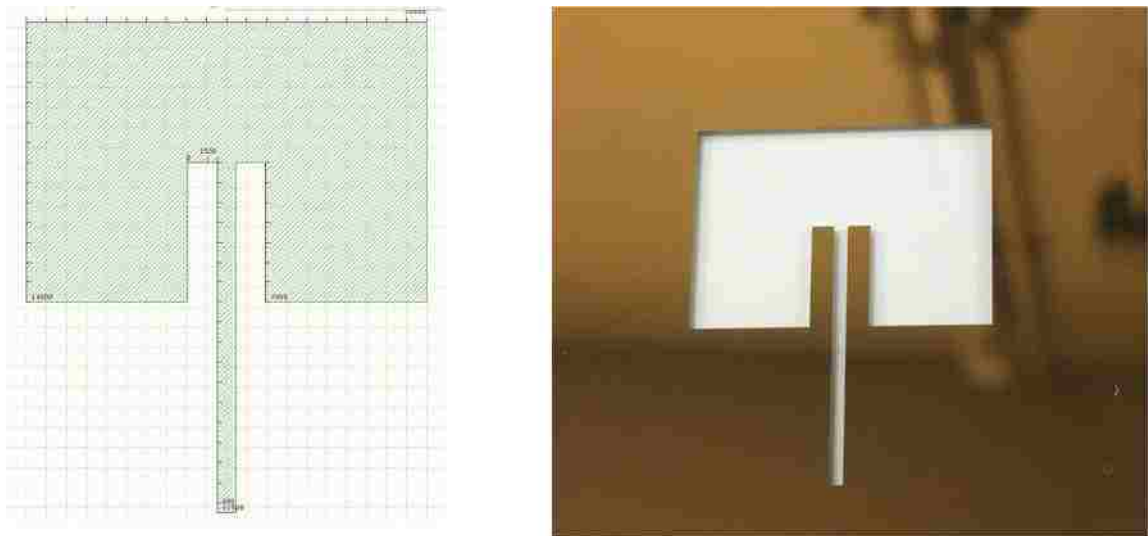
Figure 4.12 DXF file with dimensions for generating the mask (left), Mask of rectangular inset-fed patch (right).

During the photolitographic process, the sample with the AZO was covered with a photoresistor to protect the areas that were not going to be etched. In this process the negative photoresitor AZ5214EIR was used. A UV source was used next and the mask aligner used is shown in Figure 4.13. The mask was located in the mask aligner, and the sample with the photoresistor was located beneath the mask. After they were perfectly aligned the sample was exposed throught the mask to UV during 1.95 seconds.

Figure 4.13 Mask Aligner at the Center of High Technologies CHTM.

After exposure, the photoresistor was developed with the developer AZ400 1:4 during 50 seconds. The next step was to etch the antenna on the already developed AZO film. It was determined, through experimentation, that the best etchant for this antenna was BOE (buffered oxide etch), during a period of 20 secs. During the wet etching process, the parts that were not covered by

the mask were etched from the wafer. The procedure of photolytography and etching is illustrated in Figure 4.14.
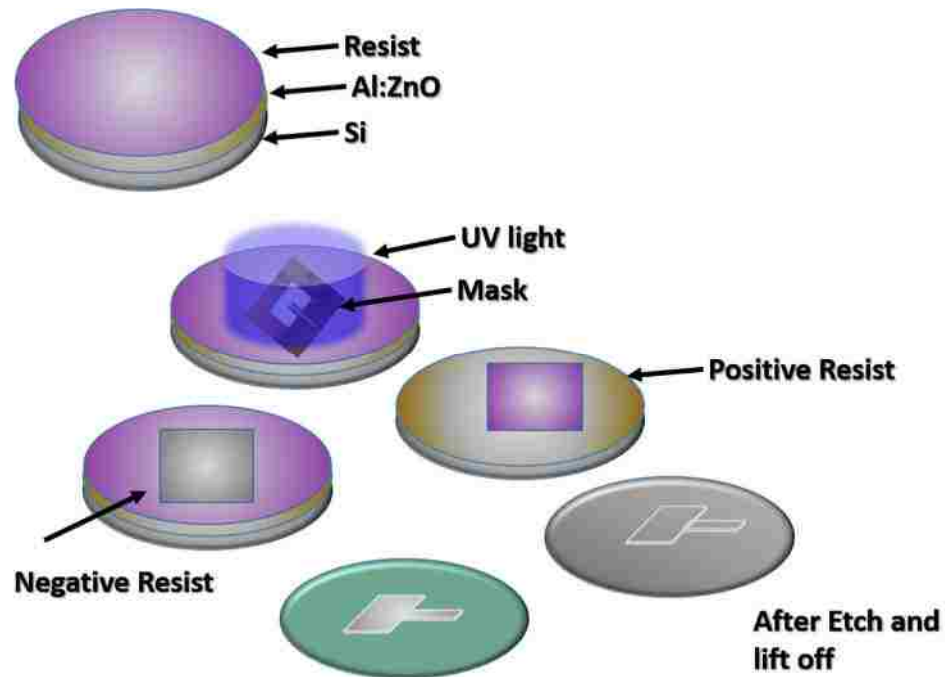
Figure 4.14 Photolithography process.

After the photolithography process the material was tested to make sure that the fabricated antenan area was accurate. To test this, two different measurements were done: One test aimed in analyzing the sample with a microscope and determine if the shape of the antenna was easy to identify.

Another test was performed on the films using a Scanning Electron Microscopy/Energy dispersive (SEM). This electron microscope uses a high-energy electron beam and generates different signals at the surface of the

samples that yield important information about the samples. This information is used to determine the chemical composition of the sample. Figure 4.15 shows the results of the process carried out on the sample inside the structure of the antenna. It was found that the sample chemical composition was made of silicon, zinc, aluminum and oxigen (the oxigen is present in ZnO). Consequently, it was determined that the fabrication process of the rectangular patch was successful.
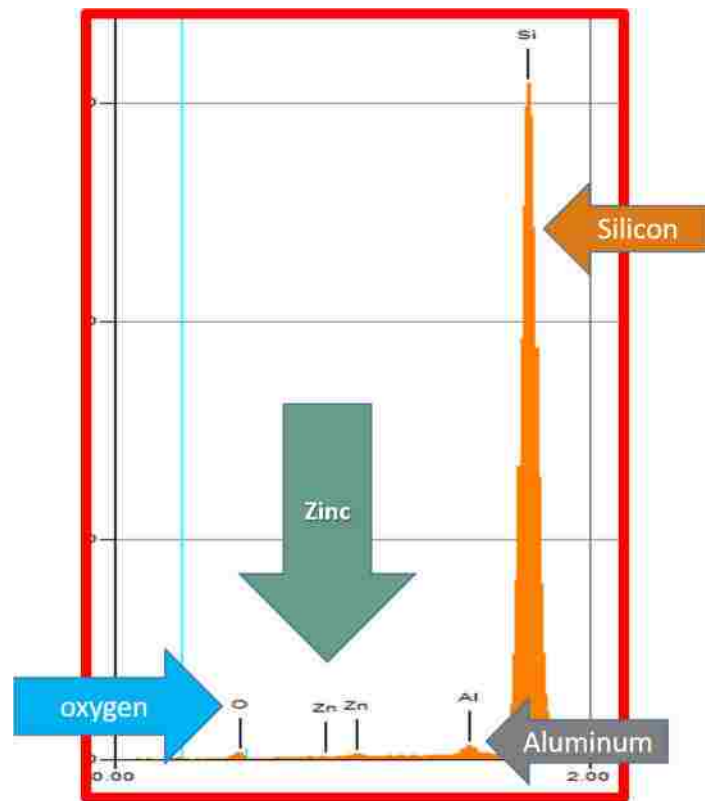
Figure 4.15 SEM results for rectangular patch antenna made with AZO film on Silicon substrate.

In order to obtain the best etched antenna, multiple antennas were fabricated and etched with the same shape and tested. Figure 4.16 shows the

antennas before and after etching. The ones in the left had still the photoresistor on top while in the picture of the right they were already etched. The blue color on the non-etched antennas picture is due the photoresistor still being present before applying the etchant.
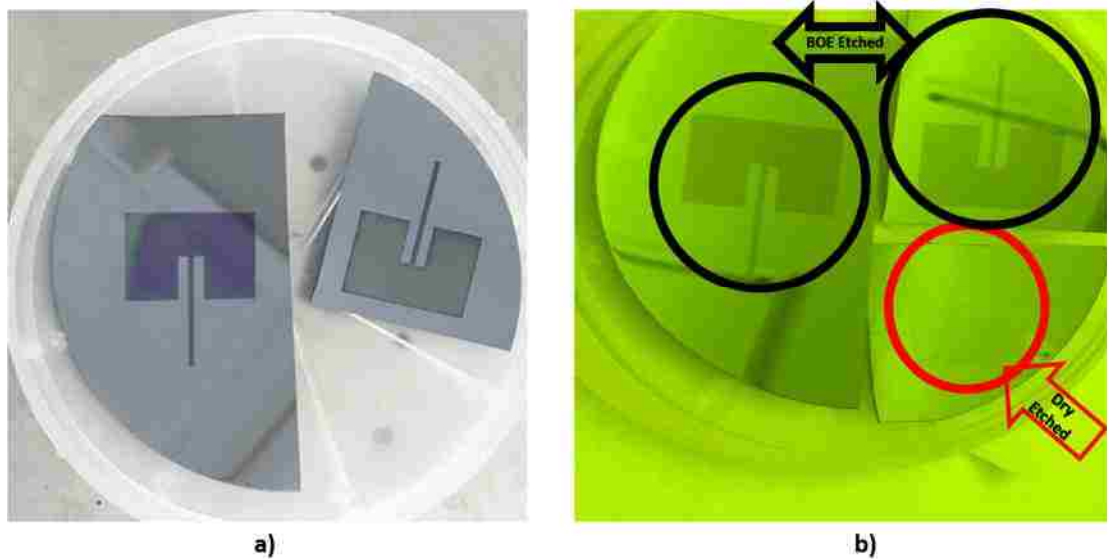
Figure 4.16 a) Antennas before etching with photoresistor, b) antennas after etching.

Different experiments were carried out to find the best etchan for the AZO material. In Figure 4.16b it is noticeable that one of the antennas shape is not very well defined. In this particular case the antenna was dry etched using an Inductively Coupled Plasma (ICP) process. The ICP process removes the material by bombarding ions to the target, i.e, AZO film samples, however, the resulting etched sample did not achieve very good quality and the shape of the antenna was hard to identify as shown in Figure 4.16 b . It was concluded that this process was not very favorable for AZO films and thus wet etching with BOE was chosen instead.

The model presented on Figure 4.11 was scaled in order to verify that the material could be used at higher frequencies. The new dimensions are: Width 20nm, length 14mm, inset-fed spacing 1.5mm, and feed line width 0.9mm. The rectangular patch AZO antenna was cold soldered to a SMA conector by means of high conductive silver epoxy, and the S-parameters were measured with the VNA PNAX N5247A.

Figure 4.17 shows the fabricated prototype a), and b) comparison between simulated and measured results of the return loss of the antenna. According to Figure 4.17, it is noticeable a slight change in the operating frequency due to losses introduced when soldering the SMA connector to the fabricated prototype. For this rectangular patch antenna the resonance frequency is 10.84GHz for the fabricated prototype, whereas for the simulation it resonates at 10.89GHz. However, the antenna shows good behavior overall, which motivated to design different antennas using AZO.

a)   b)
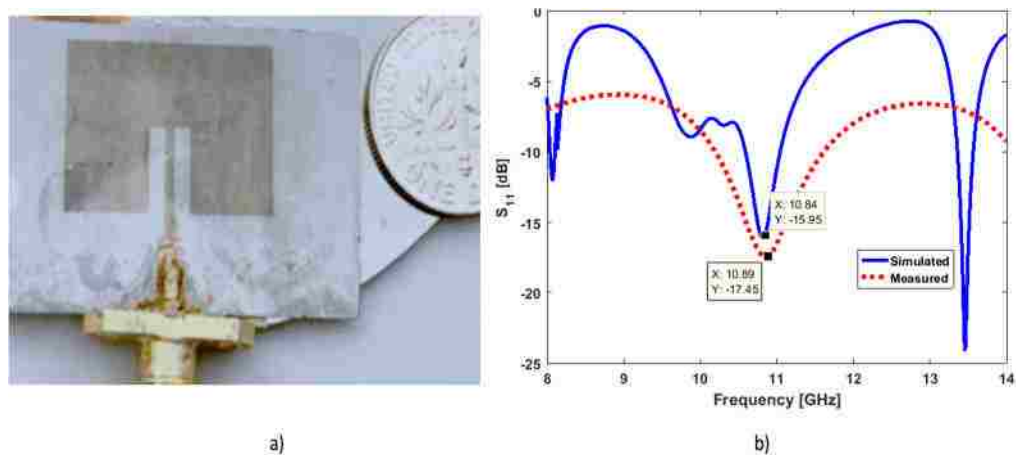
Figure 4.17 a) Fabricated prototype b) simulation, and fabricated result for return loss comparison.

The results of this antenna show that our optimized AZO film possesses good properties for efficient antenna fabrication, confirming the feasibility of the film for OTA fabrication and their integration with solar cells. Since the OTA was fabricated on top of a silicon wafer, it was demonstrated that the AZO is compatible with solar cell materials; hence the integration of solar cell-OTA by means of AZO films was proven as viable.

4.2.2. *Coplanar Waveguide (CPW) Fed Antenna*

To test the efficiency of AZO at different frequencies and with different geometries, various antenna designs were simulated, fabricated and tested. The procedure followed to fabricate and test the AZO film described in section 4.2.1 was repeated for the fabrication and testing of the antennas described in this section, and in section 4.2.4.

The design presented in Figure 4.18 consists of a coplanar waveguide CPW fed hexagonal antenna. The design was optimized to obtain the best gain. The antenna has total dimensions of $10mm x 10mm$, each ground plane has dimensions of 4.588mm, the spacing between ground planes and feeding line is 0.162mm, the feeding line width is 0.5mm, and the width of the hexagon is 4mm. These dimensions are shown in Figure 4.18 a. The conductivity used in the simulation was the average value of $\sigma = 3.98 \times 10^5 [S/cm]$ for the optimized AZO

film found in Chapter 3, with a thickness of $tf = 24nm$. The used substrate is silicon with $\varepsilon = 11.9$, and a thickness of $t = 0.37mm$.
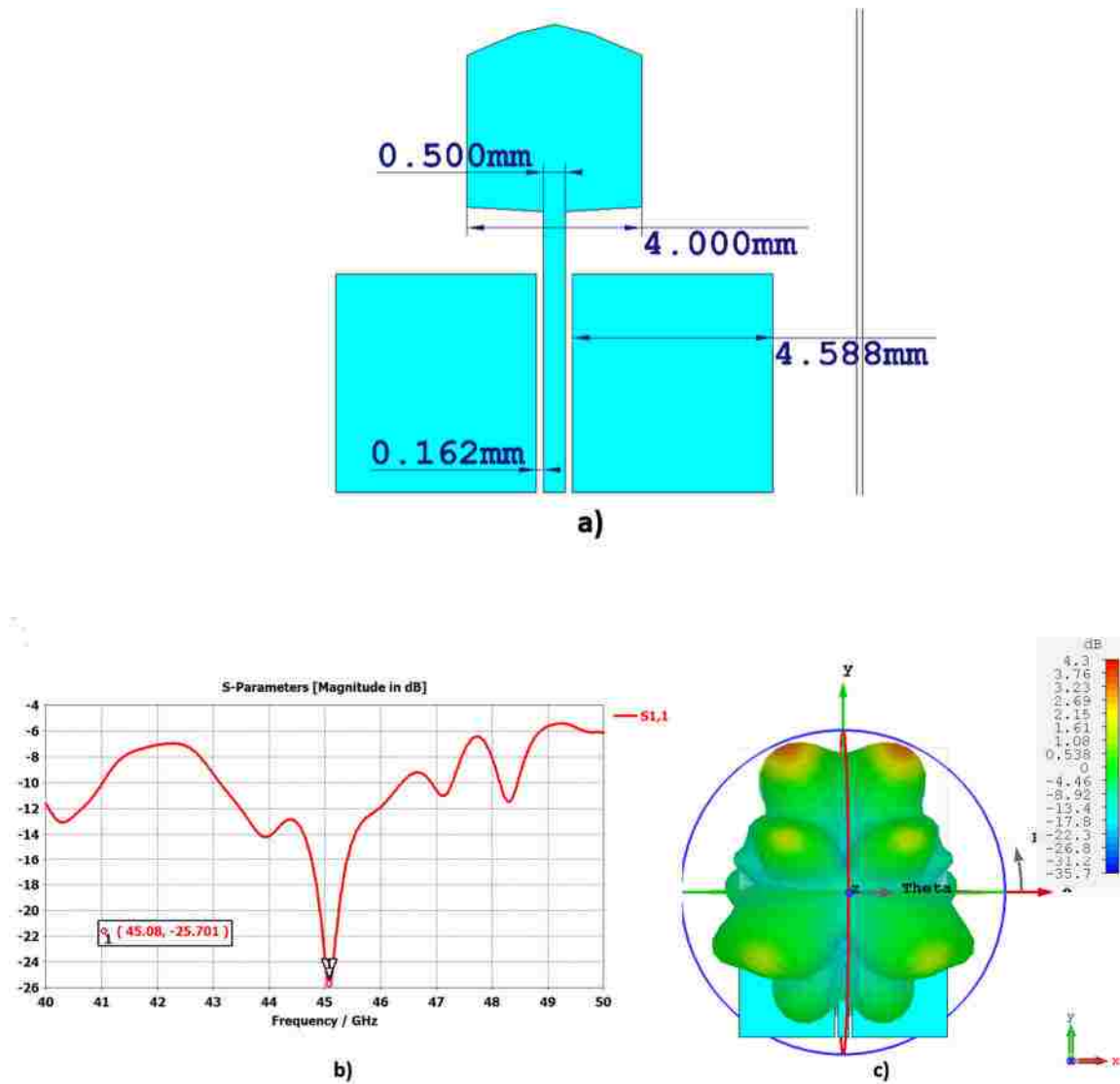
Figure 4.18 a) Hexagonal patch antenna CPW fed , b) return loss simulation, c) Gain and Radiation Pattern.

4.2.2.1. *Fabrication and Measurements of the CPW Antenna*

The CPW antenna was fabricated by employing the photolithography process described in Figure 4.14, section 4.2.1. The DXF file and generated mask are shown in Figure 4.19. Since the mask is opposite to the mask in Figure 4.12, this time it was required the use of positive photoresistor instead of the negative photoresistor described in section 4.2.1. The remaining of the process followed the same steps as for the rectangular patch; the developing and the etching of the CPW antenna were done in the exact same way as described in section 4.2.1.1 using same developer AZ400 1:4 during 50 seconds, and same BOE etchant during 20 seconds for etching.

a)   b)
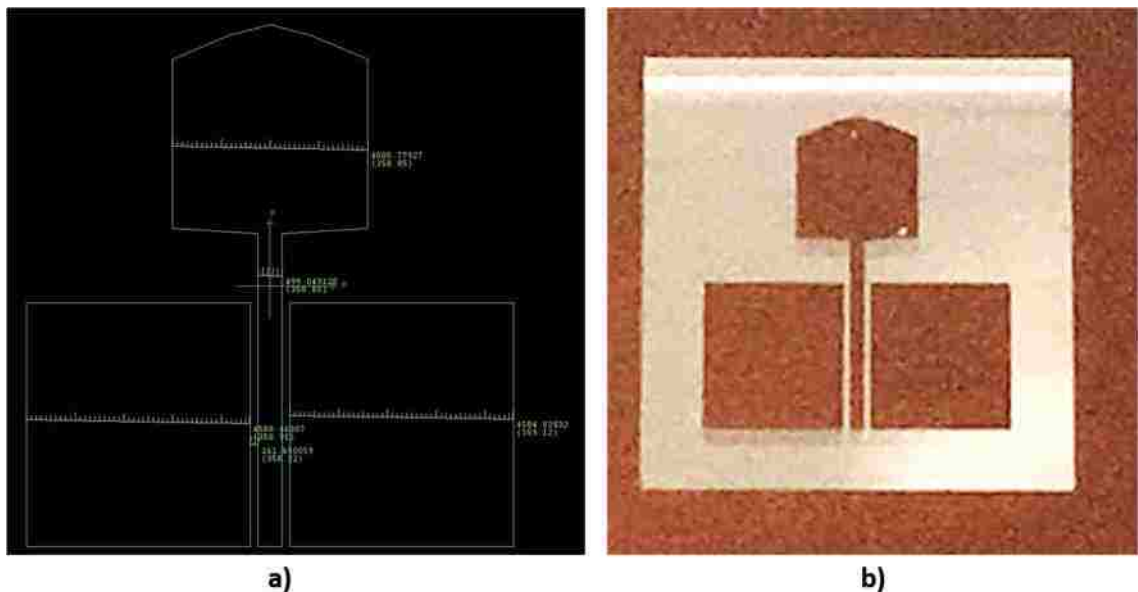
Figure 4.19 a) DXF file CPW antenna, b) generated mask.

Since the SMA connector introduced some losses on the rectangular patch antenna, the CPW antenna was designed to have the ground plane and feeding line in the same surface. Thus, it was possible to test it with a probe station, and it was not necessary to employ an SMA connector.

The measurements were done by means of the probe station Cascade Microtech MPS150. The specific probe for these measurements has a spacing of 500um. Figure 4.20 describes the calibration process of the probe. To perform the calibration it was neccesary to employ an Impedance Standard Substrate (ISS) with the specific size and requirements for a 50 Ω load, and for the short contacts. The open part of the calibration was done by separating the probe from the ISS at least 200um.
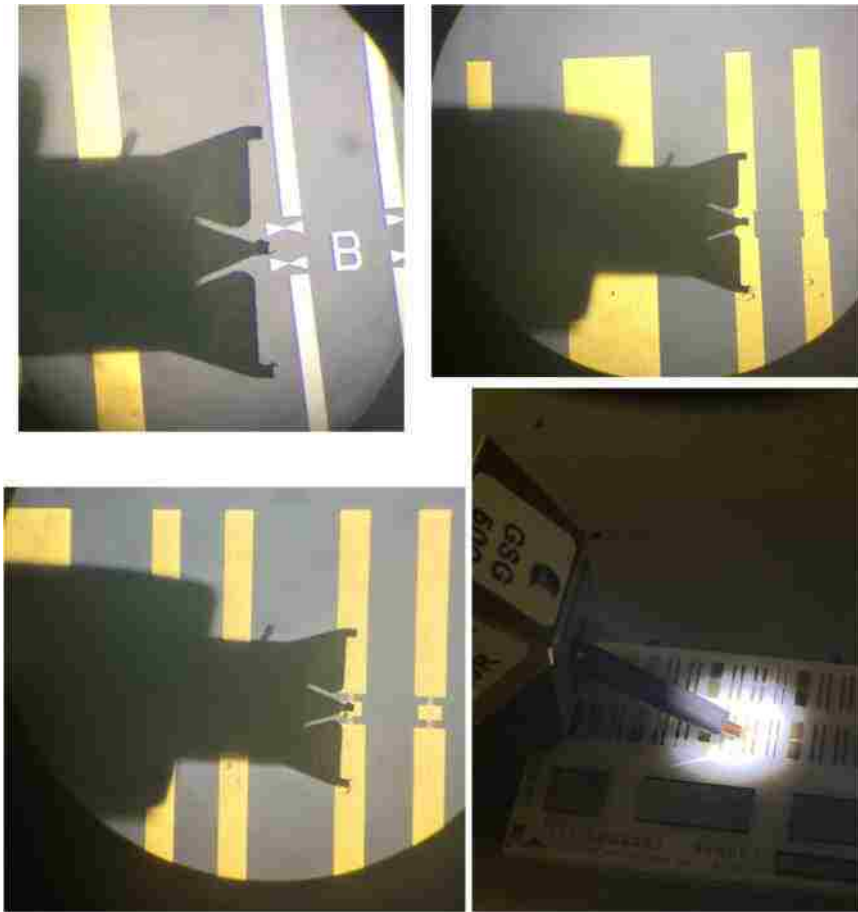
Figure 4.20 Calibration of the wide pitch probe using ISS 106-682. (Upper left) probe alignment, (upper right) short circuit calibrations, (lower left) load calibration, and (lower right) probe with ISS.

Figure 4.21 depicts the fabricated prototype of the CPW antenna (left top), the probe making the contact with the feeding and the ground plane of the antenna (bottom left). The plot with the comparison between simulated and measured return loss is shown on the right.
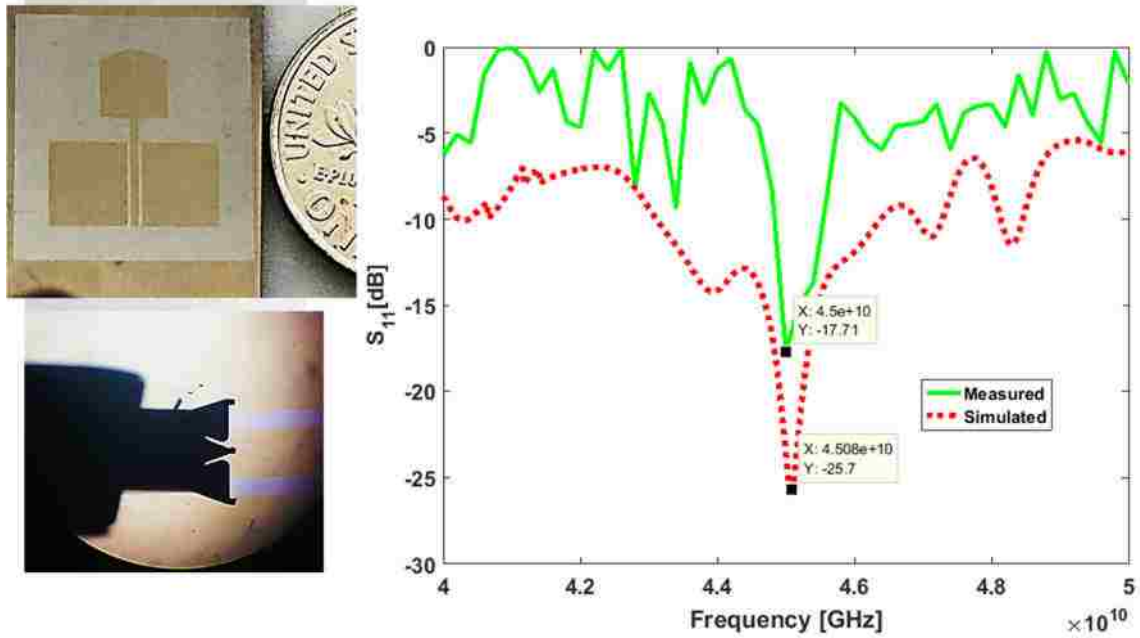
Figure 4.21 Left: Fabricated prototype (left top), probe measuring the antenna (left bottom). Right: Measured and Simulated S11.

It can be seen in Figure 4.21 that the measured and the simulated results have a good agreement in frequency. The peaks present in the measured results are due to some impurities presented on the wafer during measurement. The measured and simulated results comparison is still satisfactory, and the antenna presents good behavior overall. It is important to notice that this antenna works at very high frequencies (45 GHz) compared with the previous designs (2.4GHz and 10.84GHz), the results show that the AZO material is still feasible for very high frequency antennas.

4.2.3. _Simulation First Antenna Array_

Based on the optimized results of the AZO samples obtained previously, a two-element transparent antenna array with its entire feeding network made of AZO film was designed and simulated. The array was designed to operate at satellite communications channel frequencies as shown in Figure 4.22 a. To consider the effects of a solar cell on the antenna array performance, the silicon substrate material was chosen.
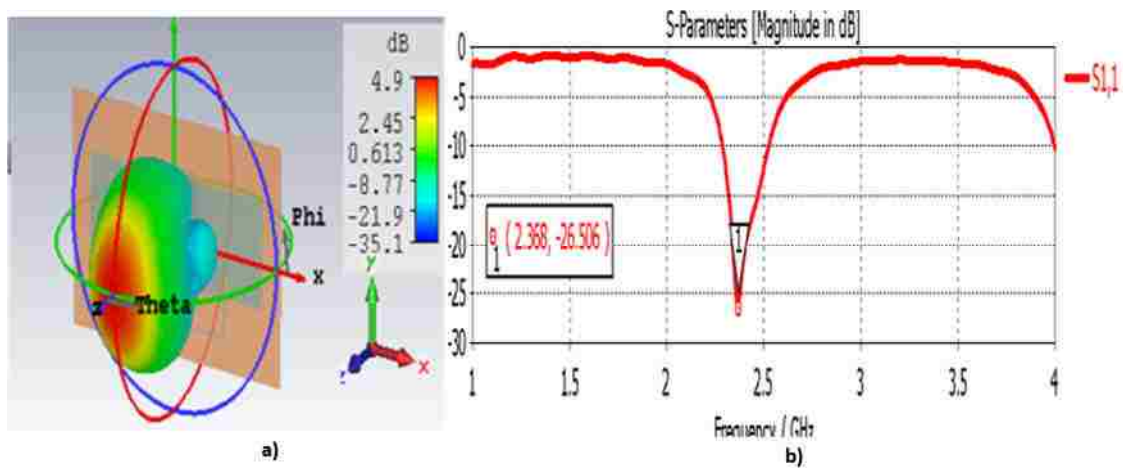
Figure 4.22 a) Array gain, and b) return loss.

The array total dimension including the feeding network was 19 cm x 13 cm. The array consisted of two rectangular inset fed patch antenna elements designed to operate at 2.4 GHz. The array realized gain is around 5 dB. The simulation result for reflection coefficient is summarized in Figure 4.22 b. These results show that the optimized AZO film presents good RF properties even for an

array antenna, therefore, it has a good potential for the design and fabrication of optically efficient transparent antennas to be integrated with solar cells.

4.2.4. *Array Fabrication*

The array design in Figure 4.22 was modified and optimized to cover higher frequencies. Figure 4.23 depicts the simulation results for the optimized antenna array designed with AZO film. The total dimension of the array are 14mm by 10 mm including its feeding network.The simulation results reflect good behavior for the array with a realized gain of 8.57dB. For the fabrication of this design, it was decided to grow the AZO film directly on top of the solar cell shown in Figure 4.25, following all the optimization processes described in Chapter 3. Four layers of AZO material were deposited, each 6nm in thickness for a total of a 24nm AZO film. same parameters were used as described in section 3.1.1, and the solar cell was annealed for 48 hours at 450°C.

a)
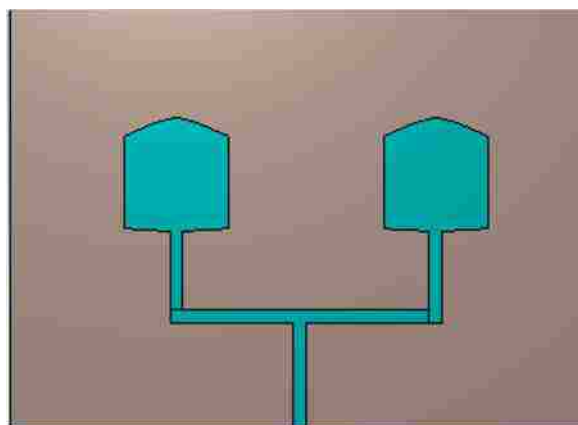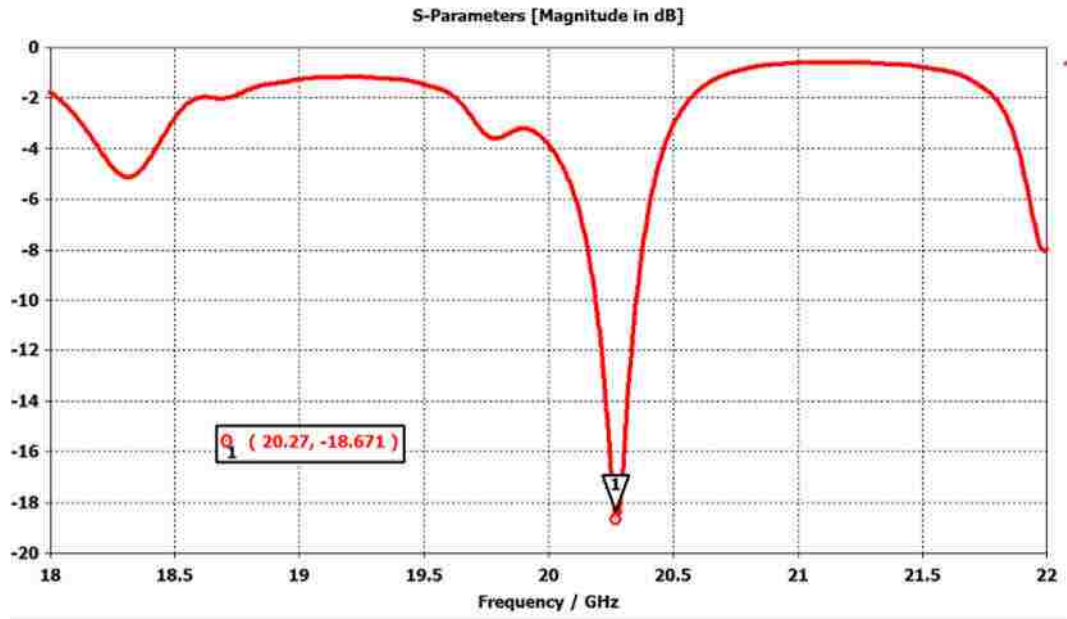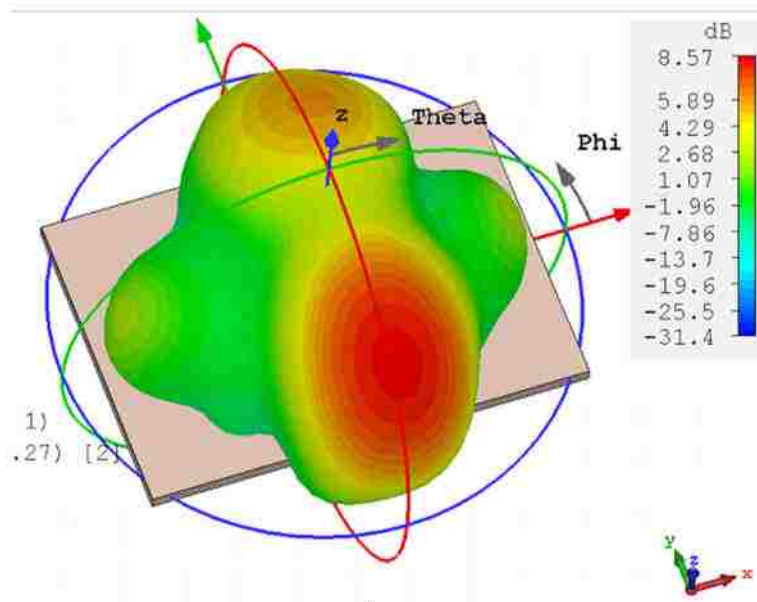
Figure 4.23 a) Two element array, b) return loss simulation, c) gain simulation.

The fabrication process for this array followed the same steps described in sections 4.2.1.1 and 4.2.2.1.The solar cell chosen for this experiment does not have any conductive contact on top of it; consequently it was possible to deposit the AZO film on top of this photovoltaic . The DXF file and the resulting mask are shown in Figure 4.24

a)   b)
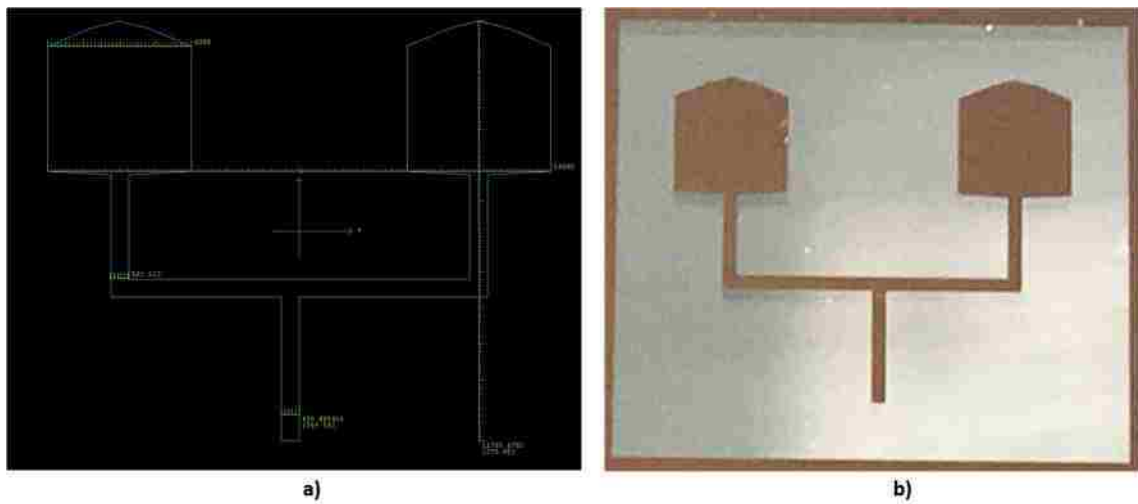
Figure 4.24 a) DXF file with dimensions and b) generated mask.

As previously mentioned, the AZO film was deposited on top of a photovoltaic.   This photovoltaic has the backside contacts with a pattern presented in Figure 4.25 b). The measurements of the antenna were proposed to be done by employing an SMA connector, and the use of cold soldering with silver epoxy to solder the SMA. To assure a good contact, a clear wax to seal the soldering was employed. However, the solar cell proved to be extremely fragile breaking multiple times during the photolithography and etching processes; yet, the array was successfully fabricated as depicted in Figure 4.25a), but the trials

or testing were compromising the physical integrity of the solar cell. Therefore, new techniques are needed to measure the S-parameters of this array.
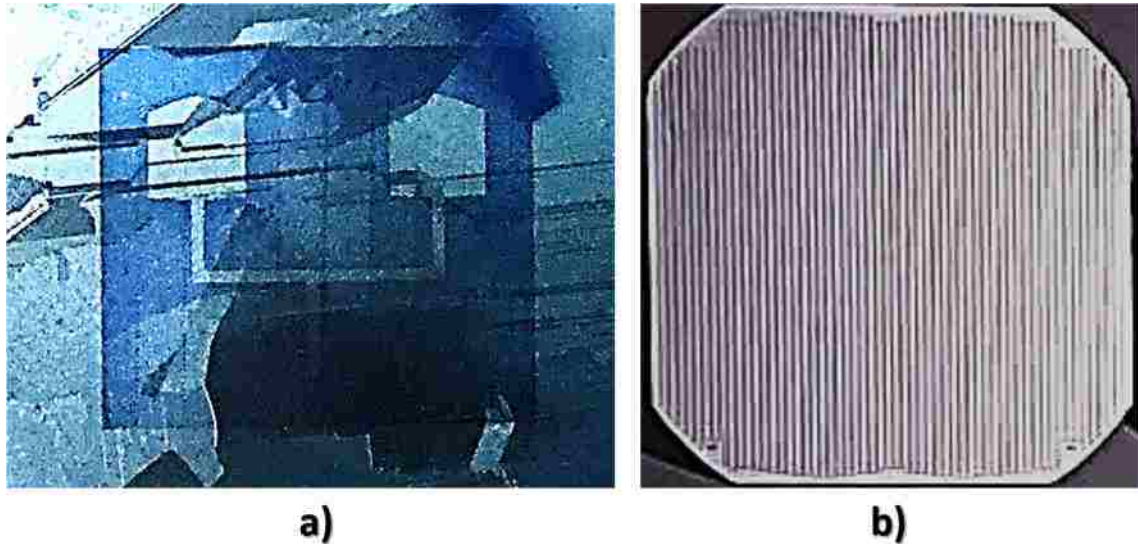
Figure 4.25 Fabricated prototype for AZO array.

Although the array could not be measured it was proven to have good behavior per the simulated data in Figure 4.23. As a conclusion, it is important to mention the overall good behavior of the AZO film for using in designing various antenna geometries. The scattering parameters were tested for these antennas confirming good agreement with the simulated results. Subsequently, the AZO optimization process was proven to be successful and most importantly it was demonstrated that it can be used for RF devices such as OTAs.

Chapter 5: Conclusions and Future Work

5.1. *Summary and Conclusions*

In this dissertation work, a new type of material, based on aluminum doped zinc oxide (AZO), for fabricating highly transparent and good conducting antennas at RF frquencies has been developed and optimized. Since these transparent antennas are to be integrated with photovoltaics, their required optical properties, their fabrication and their overall optimization process is presented and discussed. Furthermore, the analytical and experimental characterizations of this new material for transparent antennas are described and discussed in details.

The optimization process starts with the preparation of the film by sputtering thin layers of zinc oxide and aluminum oxide on a silicon (100) wafer. The material fabrication process was done at the Center for High Technology materials (CHTM) and the Center for Integrated Nanotechnology CINT.

The deposition rate and the amount of each one of the materials involved in AZO fabrication was controlled by employing different targets for each element in the film (Aluminum and Zinc Oxide). Since the light absorption can be affected by trapping effectes present when a surface is irregular, the surface of the samples was measured with a profilometer in order to obtain samples with the most smooth and uniform surface.

The obtained samples, with the material deposited, were annealed next , at different temperatures and times. The goal was to find the best temperature-time combination for the aluminum to dope the zinc oxide and to obtain higher conductivity and transmittance.

After annealing, different measurements and characterizations were done to guarantee an optimized process. The sheet resistance of the samples was measured using the four-probe technique to investigate the resulting conductivity of the samples after optimization. To assure a high transmittance level, the transmittance data was measured by means of ellypsometry and spectroscopy in the wavelenght region between 350 nm and 750 nm. This region was chosen accordingly to the best quantum efficiency of the solar cell. We noticed tha the most transparent film is the one annealed at 450°C for 48 hours reaching a percentage of transmittance of 86%.

The characterization results, show that the optimized AZO possesses good conductivity, $\sigma = 3.98 \times 10^5 [S/cm]$, and the measurements in the visible region indicate that the material has a high level of transmittance of 79% to 83%. As a result, it was determined that the optimized AZO has the required optical and RF properties for OTA design, fabrication and integration with photovoltaics.

Different OTA designs were simulated, fabricated and tested with the material resulting in good agreement between simulations and measured results. The antennas were designed for various frequency ranges to test the behavior of the material. Additionally, all simulations and measurements of the AZO film were done using a silicon wafer as substrate to consider the effects of AZO on solar

cell materials. The results of these experiments proved the feasibility of AZO for transparent antenna fabrication as well as the integration with solar cells for antennas fabricated with AZO.

Finally, as a proof of concept for the potential of AZO for OTAS integrated with photovoltaics, a two-element antenna array on top of a solar cell was simulated as well. The simulation results show that the use of AZO is possible for fabrication of optically transparent array antennas to be integrated with photovoltaics.

5.2. *Future Work*

The proposed extension of the research work undertaken in this dissertation covers the following points:

- Try different concentrations for ZnO and Al during the deposition process to test their effect on overall conductivity and transmittance performance.
- Characterize AZO for each different concentration of Aluminum and Zinc Oxide.
- Test AZO materials for space environmental conditions.
- Develop a technique to measure the antennas already integrated with photovoltaics.

- Learn different and efficient ways to feed the optically transparent antenna, assuring that this feeding will not affect the transparency of the antenna, hence the efficiency of the solar cell.

- Develop a rectena made with AZO and test the energy harvesting with the transparent antenna.

APPENDIX A

A.1   <u>Matlab code to access remotely the Agilent MXA n90201 signal analyzer</u>

```matlab
fullURL =
['http://129.24.28.36/Agilent.SA.WebInstrument/Trace1.csv' ...
          '?term=urlwrite'];
filename = 'trace1.csv';
urlwrite(fullURL,filename);
```

A.2   <u>Matlab code to set a timer and save the measurements every twenty minutes during 24 hours</u>

```matlab
Function Tracetimer
% Create and configure timer object
t = timer ('period',600);
set(t,'ExecutionMode','fixedRate', ... % Run continuously
'timerfcn',@MyTimerFcn); % Run MyTimerFcn at each timer event
counter=1;
start(t)
function MyTimerFcn(~,~)
fullURL = ['http://129.24.28.36/Agilent.SA.WebInstrument/Trace1.csv'
...
          '?term=urlwrite'];
trace='trace';
extension='.csv';
space=' ';
filename = strcat(trace,space,int2str(counter),extension);
urlwrite(fullURL,filename);
counter=counter+1;
end
end % function Tracetimer
```

APPENDIX B

B.1   *Matlab Code to Calibrate the Coaxial Probe*

```matlab
% %The integral is supposed to be used to find Gamma,the reflection
% %coefficient, for a coaxial probe for open and load calibration, in
this part I show for open
% %
clc
clear
close all
Er=2.75;
Er_o= 1;
Er_l=10.9*(1-1i*0.001);
d=6.375e-3;
Rin=0.6e-3;
Rout=2e-3;
c=3.0*10^8; %m/s
f=1e9:49e9/193:50e9;%GHz
f=f';
k0=2*pi./(f/c); %wavenumber constant free space depending on f
z=k0.*Rout; %variable for outer coax diameter and k0 used for bessel
functions
z1=k0.*Rin;%variable for inner coax diameter and k0 used for bessel
functions

% Calibration Open

syms x
A=Er_o/(sqrt(Er)*log(Rout/Rin));
q = zeros(1,length(k0));
q =q';
Y_o = zeros(1,length(k0));
Y_o=Y_o';
GA_O =zeros(1,length(k0));
GA_O=GA_O';
for jj =1:length(k0)
    Y=@(x)(((besselj(0,z(jj).*x)- besselj(0,z1(jj).*x)).^2)./x
).*(1./sqrt(Er_o-x.^2));
    q(jj)=integral(Y,0,inf);
    Y_o(jj)=A*q(jj);
    GA_O(jj)= (1 - Y_o(jj))./(1 + Y_o(jj));
end
% plot(f,real(GA_O))
% figure
% plot(f,imag(GammA_O))
```

```matlab
% figure

% plot(f,abs(GA_O))
% ylabel('Gamma Open')




% Calibration Short

GA_S= rand (-1);
GA_S(1:194, 1:1)=-1;


% Calibration Load

A_L=Er_l/(sqrt(Er)*log(Rout/Rin));
q_L = zeros(1,length(k0));
q_L=q_L';
Y_L= zeros(1,length(k0));
Y_L=Y_L';
GA_L =zeros(1,length(k0));
GA_L=GA_L';
L= zeros(1,length(k0));
% i = -sqrt(-1);
syms y
for ii =1:length(k0)
    L=@(y) 1./(sqrt(Er_l - y.^2)).*(1+exp(-1i*2*k0(ii)*d.*(sqrt(Er_l -
y.^2))))./(1-exp(-1i*2*k0(ii)*d.*(sqrt(Er_l -
y.^2)))).*(((besselj(0,z(ii).*y)- besselj(0,z1(ii).*y)).^2)./y) ;
    q_L(ii)=integral(L,0,inf);
    Y_L(ii)=A_L*q_L(ii);
    GA_L(ii)= (1-Y_L(ii))./(1 + Y_L(ii));
end
figure
plot(f,abs(GA_L))
ylabel('Gamma Load')

find a, b and c



format long

GA_O = csvread('open_Cal.csv',7,1);
GA_L = csvread('load_Cal.csv',7,1);
GA_S = csvread('short_Cal.csv',7,1);
GM_O = csvread('open.csv',7,1);
GM_L = csvread('load.csv',7,1);
GM_S = csvread('short.csv',7,1);
ABC_response = zeros(3,length(GA_O));
for ii = 1:length(GA_O);
    mat= [GA_O(ii) 1 -GA_O(ii)*GM_O(ii);...
            GA_S(ii) 1 -GA_S(ii)*GM_S(ii);...
            GA_L(ii) 1 -GA_L(ii)*GM_L(ii)];
```

```matlab
            RIGHT_mat = [GM_O(ii);...
                         GM_S(ii);...
                         GM_L(ii)];

             ABC_response(:,ii) = mat \ RIGHT_mat;
end
figure
plot(ABC_response(1,:))
hold
plot(ABC_response(2,:))
hold
plot(ABC_response(3,:))

A1 = ABC_response(1,:)';

B1 = ABC_response(2,:)';

C1 = ABC_response(3,:)';


figure
plot (A1);
hold
plot (B1);
hold
plot (C1);


For Open, find GammA_O

G_M_O=GM_O(:,1)+i.*GM_O(:,2);

GammA_O=(G_M_O-B1)./(-C1.*G_M_O+A1);

Z0=377;
E0= 8.85418782*10^-12;
f=1e9:49e9/193:50e9;%GHz
f=f';
w=2*pi.*f;
Tazo= 24e-9;
Er= 2.75;
Oazo=(1/(Tazo*Z0))*real(sqrt(Er).*((1-GammA_O)./(1+GammA_O)));
Epazo=((w.*Tazo*Z0).^-1).*imag((sqrt(Er)).*((1-GammA_O)./(1+GammA_O)));
Erazo=(Epazo-1i.*(Oazo./w))./E0;

figure
plot (f,Oazo,'-r','Linewidth',2.5);
set(gca,'Fontsize',14);
set(gcf,'color','w');
title ('conductivity');
xlabel('frequency');
ylabel('\sigma');
grid on;

figure
```

```matlab
plot (f,Epazo,'-g','Linewidth',2.5);
set(gca,'Fontsize',14);
set(gcf,'color','w');
title ('epsilon imaginary');
xlabel('frequency');
ylabel('\epsilon_{AZO}');
grid on;

figure

plot (f,Erazo,'-b','Linewidth',2.5);
set(gca,'Fontsize',14);
set(gcf,'color','w');
title ('epsilon');
xlabel('frequency');
ylabel('\epsilon_{AZO}');
grid on;

For Open, find GammA_O

G_M_O=GM_O(:,1)+i.*GM_O(:,2);

GammA_O=(G_M_O-B1)./(-C1.*G_M_O+A1);



Z0=377;
E0= 8.85418782*10^-12;
f=1e9:49e9/193:50e9;%GHz
f=f';
w=2*pi.*f;
Tazo= 24e-9;
Er= 2.75;
Oazo=(1/(Tazo*Z0))*real(sqrt(Er).*((1-GammA_O)./(1+GammA_O)));
Epazo=((w.*Tazo*Z0).^-1).*imag((sqrt(Er)).*((1-GammA_O)./(1+GammA_O)));
Erazo=(Epazo-1i.*(Oazo./w))./E0;

figure ;
plot (f,Oazo,'-r','Linewidth',2.5);
set(gca,'Fontsize',14);
set(gcf,'color','w');
title ('conductivity');
xlabel('frequency');
ylabel('\sigma');
grid on;

figure
plot (f,Epazo,'-g','Linewidth',2.5);
set(gca,'Fontsize',14);
set(gcf,'color','w');
title ('epsilon imaginary');
xlabel('frequency');
ylabel('\epsilon_{AZO}');
grid on;

figure
```

```matlab
plot (f,Erazo,'-b','Linewidth',2.5);
set(gca,'Fontsize',14);
set(gcf,'color','w');
title ('epsilon');
xlabel('frequency');
ylabel('\epsilon_{AZO}');
grid on;
```

B.2   _Matlab Code to generate the RF conductivity plots_

```matlab
clc
clear all
close all

G_M_L = csvread('open.csv',7,1);
GM_L=G_M_L(:,1)+i.*G_M_L(:,2);

Z0=377;
E0= 8.85418782*10^-12;
f=1e9:49e9/193:50e9;%GHz
f=f';
w=2*pi.*f;
Tazo= 12e-9;
Er= 2.75-(i*0.00275);
Oazo=(1/(Tazo*Z0))*real(sqrt(Er).*((1-GM_L)./(1+GM_L)));
Epazo=((w.*Tazo*Z0).^-1).*(imag(sqrt(Er).*((1-GM_L)./(1+GM_L))));
Erazo=(Epazo-((i.*Oazo./w)))./E0;

figure
plot (f,Oazo,'-r','Linewidth',2.5);
set(gca,'Fontsize',14);
set(gcf,'color','w');
title ('Conductivity ');
xlabel('Frequency [Hz]');
ylabel('\sigma [S⁄cm]');
grid on;

figure

plot (f,real(Erazo),'g', f, imag (Erazo),'-b','Linewidth',2.5);
set(gca,'Fontsize',14);
set(gcf,'color','w');
title ('Complex Permittivity');
xlabel('Frequency [Hz]');
ylabel('\epsilon_{AZO}');
legend('Re(\epsilon)','Im(\epsilon)');
grid on;
```

References

[1] T. Yasin, R. Baktur and C. Furse, "A Study on the Efficiency of Transparent Patch Antennas Designed from Conductive Oxide Films," in *IEEE Antennas and Propagation Symposium*, Spokane, Washington, 2011.

[2] R. J. Saberin and C. Furse, "Challenges with Optically Transparent Patch Antennas," in *APS-URSI 2010*, Toronto, 2012.

[3] U. S. Pushpa and S. Chopde, "An insight on Transparent Antennas," *International Journal of Modern Engineering Research,* vol. 4, no. 9, pp. 35-41, 2014.

[4] N. Guan, H. Furuya, Delaune D and K. Ito, "Antennas Made of Transparent Conductive Film," in *PIERS Preceedings Online*, 2008.

[5] T. Peter, Optically Transparent UWB Antenna for Wireless Application & Energy Harvesting, B. University, Ed., Uxbridge: PhD Dissertation, 2012.

[6] J. Lucas, "What Is Electromagnetic Radiation?," LIVESCIENCE, 2015 March 2015. [Online]. Available: http://www.livescience.com/38169-electromagnetism.html. [Accessed 26 September 2016].

[7] R. G. Gordon, "Criteria for Choosing Transparent Conductors," *Material Research Society,* pp. 52-57, August 2000.

[8] Institute of Physics, "Energy Harvesting," April 2012. [Online]. Available: http://www.iop.org/resources/energy/index.html. [Accessed 18 September 2016].

[9] J. Donovan, "Energy Harvesting for Ultra-Low-Power MCUs," Renesas, 18 September 2016. [Online]. Available: http://renesasrulz.com/doctor_micro/rx_blog/b/weblog/archive/2014/04/08/energy-harvesting-for-ultra-low-power-mcus.aspx. [Accessed 1 September 2016].

[10] School of Engineering, "Piezoelectric Materials and Applications," University of Liverpool, 11 March 2016. [Online]. Available: http://classroom.materials.ac.uk/casePiez.php. [Accessed August 2016].

[11] W. Storr, "Electronics Tutorials," 28 February 2014. [Online]. Available: http://www.electronics-tutorials.ws/diode/diode_6.html. [Accessed 9 September 2016].

[12] J. Mendoza, "Applications of Optical Phenomena," 02 March 2014 . [Online]. Available: https://prezi.com/xovzjnwwd3gg/applications-of-optical-phenomena/. [Accessed 17 October 2016].

[13] M. Polyanskiy, "Refractive Index Database," Refractive Index Info, 2008. [Online]. Available: http://refractiveindex.info/. [Accessed August 2016].

[14] T. Yasin, Transparent Antennas for Solar Cell Integration, vol. PhD Dissertation, Salt Llake City: Univesity of Utah, 2013.

[15] K. Bädeker, "Über die elektrische Leitfähigkeit und die thermoelektrische Kraft einiger Schwermetallverbindungen," *Annalen der Physik,* p. 749–766, 1907.

[16] M. Grundman, "Karl Bädeker (1877–1914) and the Discovery of Transparent Conductive Materials," *Applications and Materials Science,* vol. 212, no. 7, p. 1409–1426, 2015.

[17] C. I. Bright, "Review of Transparent Conductive Oxides TCO," *3M Company Fall Bulletin,* pp. 38-45, 2007.

[18] A. Katsounaros, Y. Hao, N. Collings and W. A. Crossland, "Optically Transparent Ultra_wideband Antenna," in *EuCap*, Berlin, 2009.

[19] T. Peter, Transparent UWB Antenna for Wireless Applications and Energy Harvesting, London: Brunel University , 2012.

[20] F. Colombel, X. Castel, M. Himdi, E. Motta-Cruz and J. Hautcoeur, "Radiofrequency Performance of Transparent Ultra-wideband Antennas," *Progress In Electromagnetics Research,* vol. 22, pp. 259-271, 2011.

[21] M. E. Zamudio, Y. Tawk, J. Costantine, F. Ayoub and C. Christodoulou, "Design of a Transparent Spiral Antenna for Energy Harvesting," in *IEEE Antennas and Propagation Symposium*, Vancouver, Ca, 2015.

[22] A. Stadler, "Transparent Conducting Oxides—An Up-To-Date Overview," *Materials,* vol. 5, no. 4, pp. 661-683, 2012.

[23] I. Hamberg and C. G. Granqvist, "Evaporated Sn-doped In2O3 Films: Basic Optical Properties and Applications to Energy-efficient Windows," *Journal of Applied Physics,* vol. 60, no. 11, p. 10.1063/1.337534, 1986.

[24] Z. Chen, W. Li, R. Li, Y. Zhang, G. Xu and H. Cheng, "Fabrication of Highly Transparent and Conductive Indium–Tin Oxide Thin Films with a High Figure of Merit via Solution Processing," *American Chemical Society,* p. 13836–13842, 11 october 2013.

[25] T. Chen and T. Cheng, "The electrical and Optical Properties of AZO Thin Film Under Different Post-annealing Temperatures," *Microsystems Technologies,* vol. 19, no. 11, p. 787–1790, 2013.

[26] H. Zhou, D. Yi, Z. Yu, L. Xiao and J. Li, "Preparation of Aluminum Doped Zinc Oxide Films and the Study of their Microstructure, Electrical and Optical Properties," *Thin Film Solid,* vol. 515, no. 17, p. 6909–6914, 2007.

[27] X. Jiang, L. Wong, M. K. Fung and S. T. Lee, "Aluminum-doped Zinc Oxide Films as Transparent Conductive Electrode for Organic Light-Emitting," *Applied Physics Letter,* vol. 83, no. 9, 2003.

[28] R. N. Simons and R. Q. Lee, "Feasibility Study of Optically Transparent Microstrip Patch Antennas," in *Antennas and Propagation Society International Symposium*, Cleveland, 1997.

[29] C. Mias, C. Tsakonas, N. Prountzos, D. C. Koutsogeorgis, S. C. Liew, C. Oswald, R. Ranson, W. M. Cranton and C. B. Thomas, "Optically Transparent Microstrip Antennas," in *IEE Colloquium on Antennas for Automotives*, London, 2000.

[30] C. Leea, C. Leeb and C. Luoa, "The Transparent Monopole Antenna for WCDMA and WLAN," in *WAMICON*, Cocoa Beach, 2006.

[31] P. Prajuabwan, S. Portnheeraphat, A. Klamchuen and J. Nukeab, "ITO Thin Films prepared by Gas-Timing RF Magnetron Sputtering for Transparent Flexible Antenna," in *Conference on Nano/Micro Engineered and Molecular Systems*, Bangkok, 2007.

[32] N. Guan, H. Furuya, K. Himeno, K. Goto and K. Ito, "A Monopole Antenna Made of a Transparent Conductive Film," in *IWAT'07*, Cambridge, 2007.

[33] N. Kirsch, A. Vacirca, E. E. Plowman, T. Kurzweg, A. Fontecchio and K. Dandekar, "Optically Transparent Conductive Polymer RFID Meandering Dipole Antenna," in *IEEE International Conference on RFID*, Orlando, 2009.

[34] J. Hautcoeur, F. Colombel, X. Castel, M. HImdi and E. Motta-Cruz, "Optically Transparent Monopole Antenna with High Radiation Efficiency Manufactured with Silver Grid Layer (AgGL)," *Electronics Letters,* vol. 45, no. 20, pp. 1014-1016, 2009.

[35] J. R. Saberin, Optically Transparent Antennas for Small Satellites, Salt Lake City: University of Utah, 2010.

[36] M. J. Roo-Ons, S. V. Shynu, M. J. Ammann, S. J. McCormacK and B. Norton, "Transparent Patch Antenna on a-Si Thin-film Glass Solar Module," *Electronics Letters,* vol. 47, no. 2, 2011.

[37] A. Porch, D. M. Morgan, R. M. Perks, M. O. Jones and P. P. Edwards, "Electromagnetic Absorption in Transparent Conducting Films," *Journal of Applied Physics,* vol. 95, no. 9, p. 10.1063/1.1689735, 2004.

[38] V. Tvarozek, S. Pavol, S. Flickyngerova, I. Novotny, P. Gaspierik, M. Netrvalova and E. Vavrinsky, "Preparation of Transparent Conductive AZO Thin Films for Solar Cells," in

Semiconductor Technologies, Bratislava, Intech, 2010, pp. 978-953-307-080-3.

[39] M. E. Zamudio, T. Busani, J. Costantine, Y. Tawk and C. Christodoulou, "Design of AZO Film for Optically Transparent Antennas," in *IEEE Antennas and Propagation Symposium*, Fajardo, Puerto Rico, 2016.

[40] N. Kerner, "Experiment II - Solution Color, Absorbance, and Beer's Law," August 2014. [Online]. Available: http://www.umich.edu/~chem125/softchalk/Exp2_Final_2/Exp2_Final_2_print.html. [Accessed January 2017].

[41] R. C. Taber, "A Parallel Plate Resonator Technique for Microwave Loss Measurements," *AIP Review of Scientific instruments,* vol. 61, no. 8, 1999.

[42] J. Baker-Jarvis, E. Vanzura and W. Kissick, "Improved technique for determining complex permittivity with the transmission/reflection methof," *IEEE transactions on microwave Theory Tech,* vol. 38, no. 8, pp. 1096-1103, 1990.

[43] C. J. Wu and T.-Y. Tseng, "Effective microwave surface impedance of superconducting films in the mixed state," *IEEE transactions Magazine,* vol. 33, no. 3, pp. 2348-2355, 1997.

[44] J.-Y. Chung , N. K. Nahar, L. Zhang, Y. Bayram, K. Sertel and J. L. Volakis, "Broadband radio frequency conductivity technique for engineered composites," *IET Microwaves, Antennas & Propagation,* vol. 6, no. 4, pp. 371-376, 2012.

[45] E. Alwan, A. Kiourti and J. L. Volakis, "Indium Tin Oxide Film Characterization at 0.1–20 GHz Using Coaxial Probe Method," *IEEE access,* vol. 3, pp. 648-652, 2015.

[46] Instruments Plastics, "New Non-Glare Finish For Conductive Film," Instruments Plastic, 20 September 2014. [Online]. Available: http://www.instrumentplastics.co.uk/news/new-non-glare-finish-for-conductive-film. [Accessed 12 January 2017].